[AMERICAN JOURNAL OF SCIENCE, VOL. 277, OCTOBER, 1977, P. 937-981]

TRANSPORT PHENOMENA IN HYDROTHERMAL SYSTEMS: COOLING PLUTONS

D. NORTON and J. KNIGHT

Department of Geosciences, University of Arizona, Tucson, Arizona 85721

ABSTRACT. The nature of heat and mass transport in pluton environments has been described by partial differential equations and simulated by numerical approximations to these equations. A series of heuristic models computed on the basis of these equations describes the general features of fluid circulation in the vicinity of an intrusive igneous body within the upper 10 km of the Earth's crust.

Analysis of these models indicates that fluid circulation is an inevitable consequence of the emplacement of magmas in the crust. The magnitude of this fluid circulation generates convective heat fluxes which predominate over conductive heat fluxes when host rock permeabilities exceed 10^{-14} cm^2. However, cooling rates for the pluton are not significantly shortened unless the pluton permeability is also $> 10^{-14}$ cm^2. The geometries of fluid circulation and isotherms are directly affected by variations in pluton size, width, level of emplacement, and permeability, as well as the distribution of permeable zones in the host rocks. Most striking, however, is the effect of the fluid properties on heat and mass transport. The overall style of fluid circulation is effectively controlled by coincident maxima of the isobaric thermal coefficient of expansion and heat capacity with the viscosity minima in the supercritical region of the H_2O-system.

Waters in natural pluton systems are predicted to move from their points of origin to positions several kilometers away in a few hundred thousand years. This redistribution affects magmatic fluids and fluids in host rocks up to several kilometers away from the pluton. Typically, temperature and pressure changes along the fluid flow paths produce dramatic changes in solvent properties. Hence, the fluid-rock interactions along the pathlines should generate diagnostic mineral assemblages and shifts in isotopic compositions. Average fluid:rock mass ratios of 0.4 are realized over the entire permeable portions of the systems.

This analysis reveals the extent of fluid circulation, and magnitude of convective heat flux over broad crustal regions and along crustal plate boundaries where igneous activity is voluminous may be much greater than heretofore realized.

INTRODUCTION

Heat and mass transport processes associated with the emplacement of magmas into the Earth's crust are continually referred to by geologists in their studies of igneous and volcanic rocks. Inferences as to the temperature and pressure conditions within the crust are made mostly on the basis of conductive heat flow, mineral stability data, and analogies to modern environments. In particular, the crystallization and cooling paths of igneous melt systems are inferred from mineral assemblages and experimentally derived phase diagrams. These methods have led to much understanding of the nature of the crust and subcrustal environment, but they require a considerable extrapolation of information derived from a rather complex process.

Magmatic processes may be described by simple physical laws which relate all relevant variables in a set of coupled partial differential equations. Such a description is appealing, primarily because it provides an analysis that is independent of traditional methods and permits consideration of the process at the crustal scale.

Emplacement of magma bodies into the Earth's crust results in large thermal perturbations which are dispersed by a combination of heat conduction and fluid circulation. Generation of a fluid potential field is

the inevitable consequence of a thermal or solute induced pore fluid density anomaly along a horizontal plane in the crust. Recognition of this fact then raises the question of the extent and nature of fluid flow associated with both thermal and "salinity" anomalies in the crust. The magnitude of fluid flux is directly related to rock permeability and transport properties of the fluid. Geophysical evidence suggests that rocks fail by fracture and have interconnected pore spaces to at least 15 km in the crust, and, therefore, convective heat transport may be considerably more significant on a crustal scale than heretofore realized.

This communication derives the partial differential equations that represent the heat transfer process associated with thermal perturbations in the crust, discusses the physical significance of these equations, presents the numerical approximations to these equations, and analyzes how geologic variations in pluton environments affect the cooling history of the pluton. A series of heuristic cooling models that demonstrate the effect of various initial and boundary values on temperature, pressure, fluid velocities, fluid pathlines, and cooling rates are presented.

Large scale fluid circulation around plutons has been actively discussed by students of mineral deposits since the earliest recognition of vein minerals (Ssu-hsiao, 1250; Van Hise, 1901; and Lindgren, 1907). Stable light isotope distribution in pluton environments suggests that fluid derived locally from the surrounding host rocks and ultimately from the local meteoric waters has circulated through most plutons (Taylor, 1971). On the basis of trace element and mineral occurrences, one predicts that a tremendous mass of fluid is required to achieve the mineralogical and bulk composition changes observed in hydrothermal systems.

Analysis of fluid circulation in the crust by mathematical methods has been a topic of study for many years. Lord Rayleigh's original work (1916) defined the fundamental problem which, together with advances in computing technology, encouraged many subsequent efforts (Wooding, 1957; Holst and Aziz, 1972; Elder, 1967; Donaldson, 1962, 1968; Lister, 1974; Ribando, Torrance, and Turcotte, 1976). The common occurrence of high salinity fluids in shallow crustal environments has also been recognized as a probable cause of fluid circulation (Nield, 1968; Veronis, 1968; Rubin, 1973). These studies have defined many of the basic governing differential equations that describe thermal and solute driven fluid circulation. However, each has dealt with idealized equations of state for the fluid and rock phases and with uniform properties in dimensionless systems. In order to relate the processes to geologic features, real fluid and rock properties have been used in this study.

Notation

a — volumetric heat sources (cal cm^{-3} $°C^{-1}$)
A — area (cm^2)
C_f — isobaric heat capacity of the fluid (cal g^{-1} $°C^{-1}$)

C_m — heat capacity at constant pressure of the media (cal g^{-1} °C^{-1})
C_p — heat capacity at constant pressure (cal g^{-1} °C^{-1})
D_1 — matrix coefficient in Poisson equation
D_2 — matrix coefficient in Poisson equation
D_3 — matrix coefficient in Poisson equation
E — internal energy (cal g^{-1})
g — gravitational force vector (cm sec^{-2})
$\bar{i}$ — unit vector in x-direction
$\bar{j}$ — unit vector in y-direction
K — η divided by k
$\bar{k}$ — unit vector in z-direction
k — permeability (cm^2)
k_m — thermal conductivity (cal (cm sec °C) $^{-1}$)
M — mass (g)
M_f — mass of fluid (g)
M_r — mass of rock (g)
P — pressure (bars)
P_r — reference pressure (bars)
q — thermodynamic heat (cal g^{-1})
q_1 — magnitude of fluid flux in x-direction (g cm^{-2} sec^{-1})
q_2 — magnitude of fluid flux in y-direction (g cm^{-2} sec^{-1})
q_3 — magnitude of fluid flux in z-direction (g cm^{-2} sec^{-1})
Q_{ADV} — nonlinear advection term
$\bar{Q}_{conduction}$ — conductive component of heat flow vector (cal cm^{-2} sec^{-1})
$\bar{Q}_{convection}$ — convective component of heat flow vector (cal cm^{-2} sec^{-1})
$\bar{Q}_n$ — component of heat flow vector normal to the surface (cal cm^{-2} sec^{-1})
Q_P — nonlinear density perturbation term
Q_{total} — total heat flux (cal sec^{-1})
$\bar{r}$ — position vector (cm)
R — arbitrary region
R_a — Rayleigh number
S — surface
t — time (sec)
T — temperature (°C)
T_o — background temperature (°C)
T_r — reference temperature (°C)
$\bar{u}$ — fluid flux vector (g cm^{-2} sec^{-1})
$\bar{u}_x$ — x-component of fluid flux vector (g cm^{-2} sec^{-1})
$\bar{u}_y$ — y-component of fluid flux vector (g cm^{-2} sec^{-1})
$\bar{u}_z$ — z-component of fluid flux vector (g cm^{-2} sec^{-1})
u — variable at known time step
u^* — variable at half time step
u^{p+1} — variable at new time step
$\bar{v}$ — velocity vector (cm sec^{-1})

or to solute content. Considering for the moment only the thermal effects and that α is not a function of temperature[1], eq (26) is integrated:

$$\rho = \rho_o \left[1 - \alpha \left(T - T_o\right)\right], \tag{27}$$

where T_o is the temperature distribution for no flow conditions. The Darcy equation for fluid flow then becomes

$$\bar{u} = \frac{-k}{\nu} \left[\rho_o \left(1 - \alpha \left(T - T_o\right) g\right) + \nabla P\right]. \tag{28}$$

The gradient in pressure with respect to the z axis is $-\rho_o g$; therefore, eq (28) becomes

$$\bar{u} = \frac{k}{\nu} \left[\alpha T - T_o) g \rho_o + \nabla_{xy} P\right]. \tag{29}$$

Eq (29) describes the mass flow due to a thermal anomaly in the Earth's crust.

Combined Equations

The energy balance, conservation of mass, and momentum equations can be treated in one of several possible ways to obtain a numerical solution. We will utilize the conservative form, where the equations are reduced to two independent scalar quantities, streamfunction and temperature.

The circulation tendency of a fluid around the surface is a vector quantity, defined as the product of the average tangential velocity and the distance around the closed surface,

$$\text{Circulation} = \bar{v}_t ds. \tag{30}$$

From Stokes Theorem we have

$$\int_S (\nabla x \, \bar{v})_n dA = \bar{v}_t ds, \tag{31}$$

where $(\nabla x \, \bar{v})_n$ is the component of $\nabla x \, \bar{v}$ in the direction of a unit vector, $\bar{n}$. Applying the circulation concept to eq (29) gives

$$\nabla x \, \frac{\nu}{k} \, \bar{u} = \nabla x \left(\alpha (T - T_o) g \rho_o\right) + \nabla x \left(\nabla_{xy} P\right) \tag{32}$$

and, since $\nabla_{x,y} P$ is a gradient field and the curl of a gradient field is zero, the fluid flow equation reduces to

$$\nabla x \, \frac{\nu}{k} \, \bar{u} - \nabla x \left(\alpha (T - T_o) g \rho_o\right) = 0. \tag{33}$$

A packet of fluid circulating through permeable rocks reacts with the enclosing rock mass and changes composition along its flow path. A description of this flow pathline is necessary to study the chemical varia-

[1] α indeed varies considerably with P and T, but this modification will be accounted for later.

tions in time of any given fluid packet. Consider a fluid packet in a permeable media and represent its position at time t_o with position vector r_i, where i denotes the particle of interest. As time varies, movement of the packet and changes in its fluid properties can be followed. The velocity of the packet is simply

$$\bar{v}_i = \frac{dr}{dt}. \tag{34}$$

Transforming to orthogonal coordinates and recalling that the fluid flow $\bar{u}$ is defined by $\bar{u} = \rho\bar{v}$,

$$\frac{\rho dx}{q_x} = \frac{\rho dy}{q_y} = \frac{\rho dz}{q_z} = dt, \tag{35}$$

where eq (35) describes the position after time increment dt.

At every instant in time, dt = 0, fluid flux vectors can be related to the streamfunction, which is tangent to these vectors. The parametric equation for this function in three dimensions is:

$$\frac{dx}{q_x} = \frac{dy}{q_y} = \frac{dz}{q_z}, \tag{36}$$

and in two dimensions eq (36) becomes

$$q_z dy - q_y dz = 0, \tag{37}$$

which is an exact differential equation since $\nabla \cdot q = 0$. Eq (37) defines the streamfunction, which can also be written as an exact differential:

$$d\Psi = \frac{\partial\Psi}{\partial y}dy + \frac{\partial\Psi}{\partial z}dz = q_z dy - q_y dz = 0. \tag{38}$$

This leads to the definition of fluid flux in terms of the streamfunction:

$$q_y = -\frac{\partial\Psi}{\partial z}\,;\; q_z = \frac{\partial\Psi}{\partial y}. \tag{39}$$

Introducing the streamfunction into eq (33) gives

$$\nabla_y x \frac{\nu}{k} \nabla_y\Psi - \nabla_z x \frac{\nu}{k} \nabla_z\Psi - \nabla_y(g\rho_o\,\alpha(T - T_o)) = 0. \tag{40}$$

Eq (40) reduces to the familiar Poisson equation: $\nabla^2\Psi = f(y,z,t)$, if ν/k is constant.

Eq (33) can now be rewritten, and the operator (∇x) expanded with respect to the y–z plane and $K = \nu/k$ substituted.

$$q_y\frac{\partial K}{\partial z} + K\frac{\partial q_y}{\partial z} - q_z\frac{\partial K}{\partial y} - K\frac{\partial q_z}{\partial y} - g\rho_o\frac{\partial(\alpha(T - T_o))}{\partial y} = 0. \tag{41}$$

Combining eq (39) with (41) and rearranging terms give the general momentum equation:

$$\nabla^2\Psi + \frac{1}{K}\frac{\partial K}{\partial z}\frac{\partial \Psi}{\partial z} + \frac{1}{K}\frac{\partial K}{\partial y}\frac{\partial \Psi}{\partial y} = \frac{g\rho_o\partial(\alpha(T - T_o))}{K\,\partial y} \tag{42}$$

Eq (42) is equivalent to

$$\frac{1}{K}\nabla \cdot (K\,\nabla\Psi) = \frac{\rho_o g\partial(\alpha T - T_o)}{K\,\partial y}, \tag{43}$$

which forms the basis of the numerical computation. Extensions to afford for anisotropic and heterogeneous permeability distribution follow directly from eq (40).

In summary, the governing partial differential equations are:

Conservation of Energy:

$$(C_m\rho_m + a)\frac{\partial T}{\partial t} + \bar{u}\nabla \cdot C_f T = \nabla \cdot (k_m \nabla T) \tag{22}$$

Conservation of Mass:

$$\nabla \cdot q = 0 \tag{21}$$

Conservation of Momentum:

$$\nabla^2\Psi + \frac{1}{K}\frac{\partial K}{\partial z}\frac{\partial \Psi}{\partial z} + \frac{1}{K}\frac{\partial K}{\partial y}\frac{\partial \Psi}{\partial y} = \frac{g\rho_o\partial(\alpha(T - T_o))}{K\,\partial y} \tag{42}$$

Dimensionless Forms of Equations

The governing equations contain three dependent quantities — temperature, streamfunction, and fluid flux. The solution can be obtained with eqs (22) and (42) alone, since eq (42) is written in conservative form, that is, eq (42) implicitly includes eq (21). In turn, fluid flux can be computed from the stream function, eq (39).

Modeling of geologic processes with the governing equations derived above requires that the variables be scaled, similar to bench scale model experiments. Scaling permits simulation of processes that occur over hundreds of thousands of years in a few minutes of computer time. Often only the dimensionless variables are reported, generally as a constant Rayleigh number; however, to afford for the equations of state of the fluid and rock utilized in this study, Rayleigh numbers were computed from actual temperatures and pressures at each time increment.

The dimensionless forms of eqs (22) and (42) (see table 1 for definitions) are

$$F\frac{\partial T}{\partial t} + \bar{u}\,\nabla C_t\,T = \nabla \cdot k_m \nabla T \tag{44}$$

$$\frac{1}{K}\nabla \cdot (K\,\nabla\,\Psi) = R_a\,\nabla\,\alpha\,T. \tag{45}$$

TABLE 1
Dimensionless and characteristic values

$y = yl^*$	$k = \underline{k}\, k^*$
$z = zl^*$	$\nu = \underline{\nu}\, \nu^*$
$\nabla = (\underline{\nabla}/l^*)$	$C_f = C_f\, C_f^*$
$T = TT^*$	$k_m = k_m\, k_m^*$
	$F = 1 + \frac{a}{\rho_m C_m}$
	$Ra = \frac{g k \rho_o C_f^* T^* \alpha^* l^*}{\nu k_m^*}$
$t = \frac{t\, l^{*2} \rho_m C_m}{k_m^*}$	$\alpha = \underline{\alpha}\, \alpha^*$
$\bar{u} = \bar{u}\, \frac{k_m^*}{C_f^*\, l^*}$	
$\Psi = \underline{\Psi}\, \frac{k_m^*}{C_f^*}$	

Starred quantities are characteristic values for the respective parameters; l^* is characteristic height. For all model systems in this paper, $\Psi = \underline{\Psi}\ 3 \times 10^{-4}$ g cm^{-1} s^{-1}.

Approximations of Equations

The dimensionless energy and momentum equations are of the general form

$$\frac{1}{K} (\nabla \cdot (C \nabla u)) = F \frac{\partial u}{\partial t} - s \tag{46}$$

where s is the nonlinear advection term in the energy equation or the density perturbation term in the momentum equations, and F is a term in the energy equation that accounts for energy sources or sinks in the domain but is equal to 1 in the momentum equation. The equation is readily solved by the alternating direction implicit method (Peaceman-Rachford, 1955).

For i = 2 this equation gives

$$u_{ij} = \gamma_{s_{2j}} + \frac{\gamma_{2_{2j}}}{2\Delta z}\, u^*_{3j}\left(\gamma_{1_{2j}} + \frac{\gamma_{2_{2j}}}{2\Delta z}\right)^{-1} \tag{55}$$

which may be substituted directly into eq (49).

Convergence and Time Steps

The numerical approximation for eq (22) is of the form

$$\nabla \cdot (k_m \nabla T) = F \frac{\partial T}{\partial t} - s. \tag{56}$$

This requires K_{ij} in numerical eq (46) to be equal to 1. A minor modification of eq (46) gives a solution to momentum eq (45) where $K = \nu/k$ and $C = \nu/k$. The transient term does not appear since energy and momentum equations are coupled, and the time step is made through the energy equation. We, therefore, require a steady-state solution which can be achieved through the relaxation sequence, used by Peaceman and Rachford (1955).

The maximum time step that will produce a convergent and stable numerical solution to the equations has been determined by stability analysis. This analysis shows the numerical solutions are stable, if time increments are constrained by

$$\Delta t < \frac{2}{\Delta z} + \frac{2}{\Delta y} + \frac{|q_z|}{\Delta z} + \frac{|q_y|}{\Delta y}. \tag{57}$$

This step size criteria returns a perfectly stable solution and is used in the steady state iteration to define the maximum step size possible for a given problem (Roache, 1972).

The numerical reliability of the model calculations was checked against analytical functions for pure conductive heat transport and were found to be in reasonable agreement. Exact verification is not possible for complex geometries of the heat source or for the combined convective-conductive heat transfer, since exact analytical solutions to these problems are impossible. The models give reasonable cooling times with respect to pure conduction, and the computed fluid fluxes seem realistic. However, the geologic reliability is entirely dependent on the reliability of the initial and boundary conditions and the equations of state for fluid and rock.

Equations of state.—Any equation of state can be used in conjunction with the numerical equations to represent rock and fluid properties. In this study the fluid properties were approximated by the H_2O–system, and the rock properties by average values for the appropriate rock composition.

Fluid.—The fluid phase transport properties significantly affect the nature of the cooling process. The fluid properties, except for viscosity, were computed directly from equations of state for the H_2O system

which was originally developed by Keenan and Keyes (1969), programmed and provided to us by Helgeson (see Helgeson and Kirkham, 1974, for details). The viscosity values were obtained from equations and tables modified from Bruges, Latto, and Ray (1966).

Rock.—The properties of the permeable media were estimated from standard table values for igneous and sedimentary rocks (Clark, 1966). Permeability data were estimated on the basis of analytical equations which relate fracture frequency and aperture to rock permeability (Norton and Knapp, 1977) and observations (Villas, 1975). The greatest uncertainty between the computed models and actual geologic processes is the woefully inadequate data on rock permeabilities. Bulk rock density and heat capacity are considered constant.

Analyses of Pluton Environments

Heat and mass transport phenomena in pluton environments depend on variations in pluton geometry, rock permeabilities, initial pluton temperature and heat content, fluid properties, and the system boundaries. Effects of these geologic parameters on the cooling process have been analyzed, using the partial differential equations and numerical approximations described above. In a sense, a sequence of heat transport experiments which simulate hypothetical systems have been computed in order to ascertain the effects of various geological parameters on transport phenomena in complex and realistic systems.

The emplacement of an igneous mass into the upper 10 km of the crust was assumed to be rapid with respect to the loss of heat by the body. The assumption was also made that fluid properties in these systems may be approximated by the equation of state for the H_2O–system, even though evidence suggests multicomponent fluids are certainly present. Circulating fluids are assumed not to react with the enclosing host rocks even though geologic evidence suggests that reactions occur. Finally, the two-dimensional domain, represented by 200 to 400 discrete points, is assumed to approximate a vertical section through the actual system. The errors introduced by the numerical approximations to the differential equations are on the order of $(\Delta z^2 + \Delta y^2)$ in space and Δt^2 in time. Overall, these errors in the model system are estimated to be less than 10 percent for the first derivatives, with respect to space and time.

The dependent variables, temperature, streamfunction, pressure, fluid, and heat flux, have been computed for a series of optimized steady state iterations which approximate the transient behavior of the system. Fluid redistribution caused by the cooling process and the temperature-pressure path that these fluids are subjected to is also summarized for a series of heuristic models, P1-P8.

Permeability.—Heat is transported in pluton environments by fluid convection and by thermal conduction. In the first portion of this communication, fluid circulation was shown to be an inevitable consequence of emplacement of dikes, stocks, and batholiths into fluid bearing host rocks. Although the magnitude of the thermal flux in such systems is a

linear function of rock permeability for low fluxes, it becomes nonlinear in systems that more closely approximate pluton environments. Therefore, relative contributions of conductive and convective heat transfer to the cooling process were compared.

The magnitude, distribution, and variation of bulk rock permeability with time affect the nature of heat transfer in the model systems. Permeability data on fractured crystalline rocks are not available; therefore, estimates have been based on a simple planar fracture model and on field observations. These considerations, together with interpretations of electrical resistivity and seismic data measured on the upper crust, indicated that bulk rock permeabilities were large enough to permit fluid circulation around hot plutons to depths of 10 to 20 km (Norton and Knapp, 1977). Therefore, we analyzed a sequence of systems whose initial conditions covered a reasonable range in bulk rock permeabilities.

Magnitude.—Systems in which host rocks have permeabilities of 10^{-17} cm^2, nanodarcy, or smaller and are saturated with a fluid whose properties are approximated by the H_2O–system apparently cool by pure conductive heat transfer since the fluid fluxes are $< 10^{-9}$ g cm^{-2} sec^{-1}. Pluton model P1 (fig. 1) is analogous to these types of systems.

Conductive heat transfer from a pluton produces isotherms that tend to be subparallel to the side and top contacts of the pluton and that have a broad convex upward form in rocks above the plutons. As we shall demonstrate in subsequent models, this pattern is unique to a system dominated by pure conductive cooling. The maximum vertical conductive heat flux is realized at the top contact between the pluton and host rocks at time = 0 yrs and decreases exponentially with increasing time (fig. 2).

The temperature maxima migrates upward from the P1 pluton top at 2 cm/yr during the initial 5×10^4 yrs and decreases to 0.5 cm/yr at 2×10^5 yrs (fig. 3). Thus, the initial condition of instantaneous emplacement of the pluton is reasonable for plutons that intrude into the upper crust at a rate $\geq$ 2 cm/yr. As a result of the relatively slow upward migration of thermal energy from the pluton, the 50°C isotherm is not displaced until 5×10^5 yrs after emplacement. Thermal decay of P1 is similar to the thermal decay predicted by Lovering (1935) and Jaeger (1968) using analytic solutions of the heat conduction equation. Their solutions predict the average pluton temperature decreases to 0.3 of the initial anomaly at 5.8×10^6 yrs, whereas our model predicts a decrease to 0.2 of the initial anomaly. The discrepancy is due to heat loss through the pluton top in our model, which was not accounted for in their analytic models, and, undoubtedly, to numerical differences.

The transition from conduction to convection dominated heat transfer occurs in systems where the fluid flux is $\gtrsim 10^{-8}$ g/cm^2 sec, if the heat content of the fluid is $\sim$ 100 cal/g. Host rock permeabilities $> 10^{-14}$ cm^2 and several kilometers tall thermal perturbations produce this magnitude of fluid flux. Models P2 and P3 demonstrate the transition

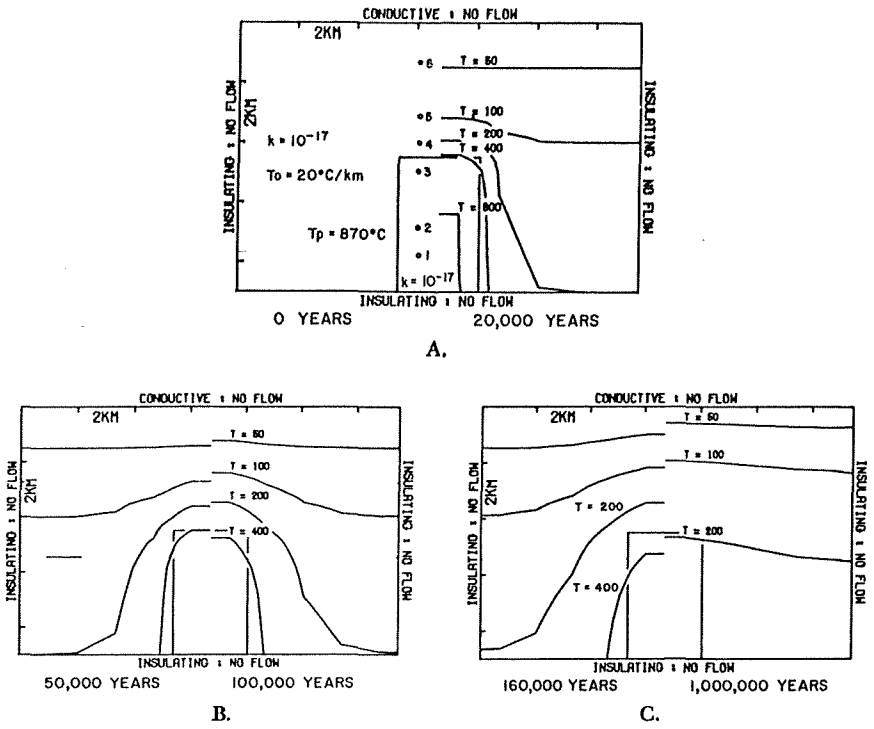

Fig. 1. Two-dimensional cross section of a pluton, Pl, and surrounding host rocks. (A) Boundary conditions and (left) initial conditions are depicted for an impermeable pluton emplaced at 870°C into uniform permeability host rocks, $k = 10^{-17}$ cm². Initial temperatures of the host rocks were defined by 20°C temperature at the top boundary and a thermal gradient of 20°C/km. The domain was represented by 100 grid points at regular intervals, $\Delta z = 0.9$ km and $\Delta y = 1.35$ km, and the cooling process was approximated by equations in text at discrete time intervals. (A) Steady state temperature distribution (right half) at elapsed time of 2×10^4 yrs. (B) Steady state temperature distribution in Pl at elapsed times of 5×10^4 yrs (left) and 10^5 yrs (right), (C) Steady temperature distribution in Pl at elapsed times of 1.6×10^5 yrs (left) and 10^6 yrs (right). Note that sharp inflections in all contoured functions are a consequence of the discretization interval and the interpolation function used in the contouring algorithm.

from conductive to convective dominated heat transport for systems containing impermeable plutons and uniformly permeable host rocks.

P2 is characterized by a host rock permeability equal to 10^{-14} cm² and has a total heat flux at the pluton top, which is on the average 10 percent greater than in Pl, although the differences in isotherm distributions in the two systems are barely discernible. Vertical convective heat flux in P2 increases from zero at $t = 0$ to 0.5 HFU at 5×10^3 yrs, remains at this value until 10^5 yrs, then decreases gradually to 0.1 HFU at 2×10^5 yrs. Systems with permeabilities $> 10^{-14}$ cm² or with taller thermal anomalies than P2 are characterized by larger convective thermal fluxes because of the direct dependence of fluid flux on vertical extent of the initial anomaly and permeability.

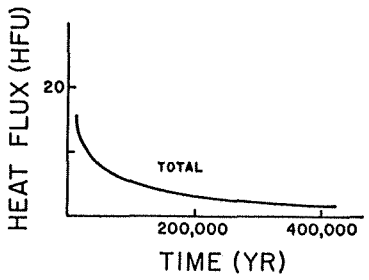

Fig. 2. Conductive heat flux in Pl as a function of time at top of pluton, 1 HFU = 10^{-6} cal cm^{-2} sec^{-1}. Thermal conductivity of 3×10^{-3} cal cm^{-1} sec^{-1} $°C^{-1}$ was assumed for all rocks in the system.

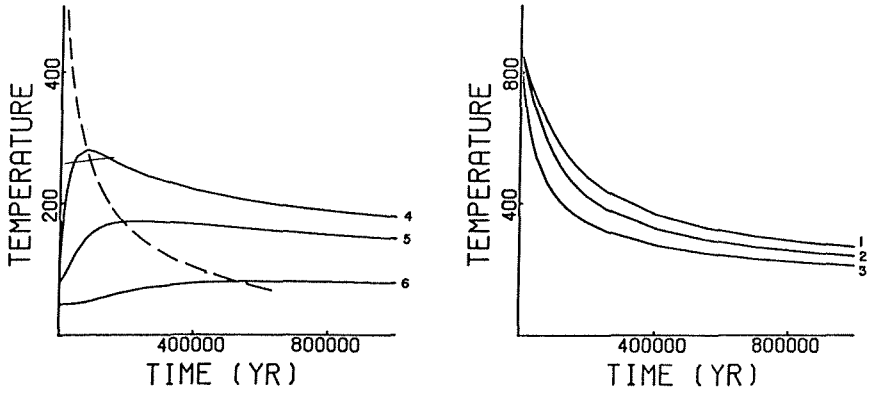

Fig. 3. Temperature as a function of time in Pl at fixed positions (left) 4, 5, and 6, fig. 1A, above top of pluton, 0.45, 1.4, and 3.2 km, respectively, and (right) within pluton at positions 1, 2, and 3, below top of pluton, 2.3, 1.4, and 0.45 km, respectively. Dashed line defines upward migration of temperature maxima with time.

Permeabilities in host rocks and plutons of 10^{-11} and 10^{-14} cm^2, respectively, cause convection to dominate the heat transfer process, P3 (fig. 4).

Fluid circulation in P3 is restricted to host rocks adjacent to and above the side contacts of the pluton (left half of fig. 4, B–D). The relatively lower permeability pluton acts as a barrier to fluid flow (left half of fig. 4B and table 2).[2]

Thermal energy is transferred upward into the overlying host rocks as the fluid circulation cells shift upward (fig. 4B–D). Although the streamfunction reaches a maximum at $\sim 10^5$ yrs, (fig. 4C), the gradient in the streamfunction near the symmetry plane of the system and at the side contacts of the pluton is a maximum at 1.6×10^5 yrs. The maximum fluxes range from 1 to 40×10^{-8} g/cm^2 sec (table 1) and occur directly above the pluton where T~300°C and P~250 bars. Although these fluid

[2] As defined in eq (40), the streamfunction is tangent to the instantaneous fluid flux vectors, and the gradient in the streamfunction defines the mass flux normal to that gradient.

A.

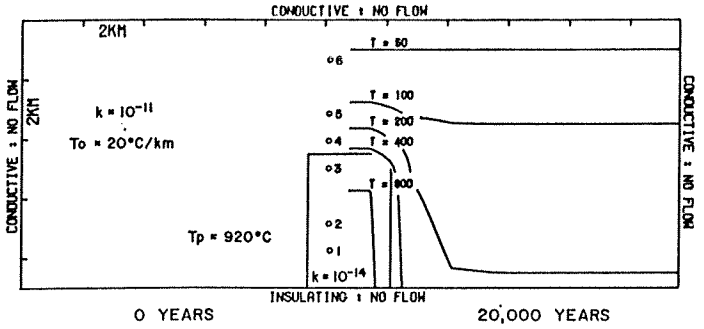
CONDUCTIVE : NO FLOW
2KM
T = 50
T = 100
T = 200
T = 400
T = 800
k = 10⁻¹¹
To = 20°C/km
Tp = 920°C
k = 10⁻¹⁴
CONDUCTIVE : NO FLOW
2KM
CONDUCTIVE : NO FLOW
INSULATING : NO FLOW
0 YEARS
20,000 YEARS

B.

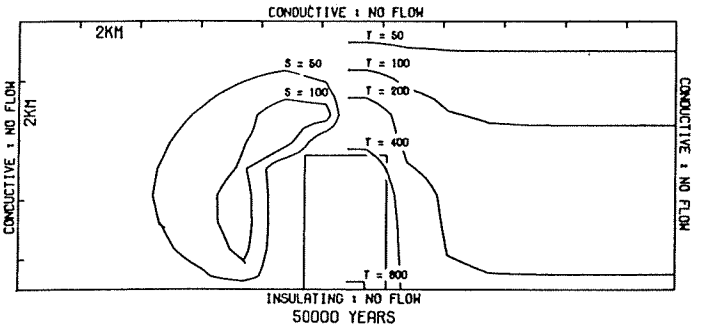
CONDUCTIVE : NO FLOW
2KM
T = 50
S = 50
T = 100
S = 100
T = 200
T = 400
T = 800
CONDUCTIVE : NO FLOW
2KM
CONDUCTIVE : NO FLOW
INSULATING : NO FLOW
50000 YEARS

C.

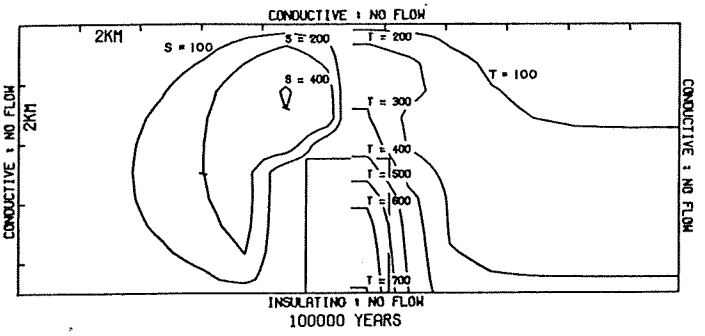
CONDUCTIVE : NO FLOW
2KM
S = 100
S = 200
T = 200
T = 100
S = 400
T = 300
T = 400
T = 500
T = 600
T = 700
CONDUCTIVE : NO FLOW
2KM
CONDUCTIVE : NO FLOW
INSULATING : NO FLOW
100000 YEARS

D.

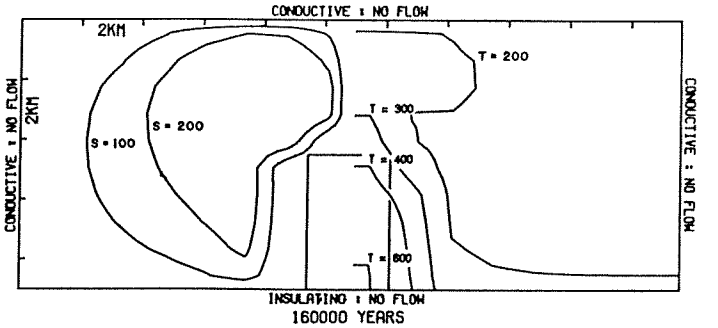
CONDUCTIVE : NO FLOW
2KM
T = 200
T = 300
S = 100
S = 200
T = 400
T = 600
CONDUCTIVE : NO FLOW
2KM
CONDUCTIVE : NO FLOW
INSULATING : NO FLOW
160000 YEARS

Fig. 4.

TABLE 2

Fluid fluxes in P3 (g cm^{-2} sec^{-1} $\times$ 10^8)

Position	time yrs =	2×10^4	5×10^4	1.6×10^5
Side contact (lower 3.6 km)				
q_y		0.07	1.	1.
q_z		5	12	25
Above top contact				
q_y		3	21	40
q_z		7	14	31

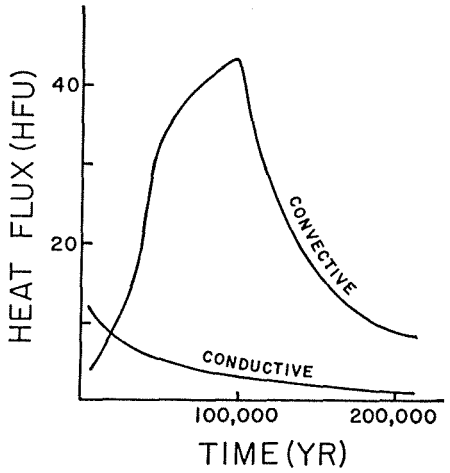

Fig. 5. Conductive and convective heat flux in P3 as a function of time at top of pluton. Thermal conductivity of 3×10^{-3} cal cm^{-1} sec^{-1} $°C^{-1}$ was used for all rocks, whereas heat capacity of fluid was determined from temperature, pressure, and the equation of state for H_2O.

fluxes are relatively small compared with shallow groundwater systems, where fluxes are 10^{-4} cm sec^{-1}, the persistence of the hydrothermal system over 2×10^5 yrs results in the circulation of a large total fluid mass.

Heat flux is directly related to the magnitude of fluid circulation. Although within the pluton heat transfer is by conduction, along the pluton margins and in the overlying host rocks convection predominates. Conductive flux at the pluton top is largest at $t = 0$ yrs and decreases with time (fig. 5). Convective flux increases from zero at $t = 0$ to a maximum of 45 HFU at slightly less than 10^5 yrs, then decreases to 10 HFU

← Fig. 4. Two-dimensional cross section of system P3 depicting boundary conditions and (left): (A) initial conditions for pluton emplaced, at an initial temperature of 920°C, into uniform permeability, $k = 10^{-11}$ cm^2, host rocks. Pluton permeability is set at maximum permeability at which conduction dominates heat transfer out of the pluton. Initial temperatures of host rocks were defined by 20°C temperature at the top boundary and a thermal gradient of 20°C/km. The domain was represented by 200 grid points at regular intervals, $\Delta z = 0.9$ km and $\Delta y = 1.35$ km. (B–D) Steady state dimensionless streamfunction representing counter-clockwise fluid circulation at (B) 5×10^4 yrs, (C) 10^5 yrs, (D) 1.6×10^5 yrs; (right) temperature distribution at (A) 2×10^4 yrs, (B) 5×10^4 yrs, (C) 10^5 yrs, (D) 1.6×10^5 yrs.

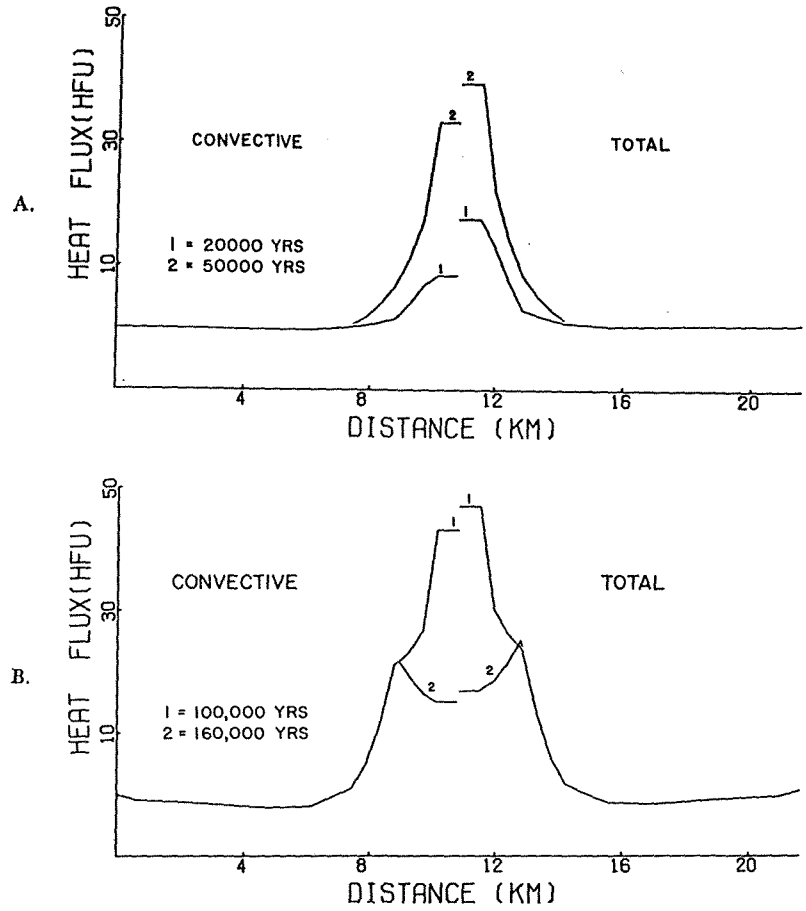

Fig. 6. Vertical component of convective and total heat fluxes as a function of distance along a horizontal plane coincident with the top of P3 pluton at elapsed times of (A) 2×10^4 yrs and 5×10^4 yrs, and (B) 10^5 yrs and 1.6×10^5 yrs.

at 2×10^5 yrs. The total heat flux across the pluton top decreases as the top portion cools. However, the large thermal gradient associated with the side contacts maintains the large heat flux in this region (fig. 6).

Convective heat flux is a nonlinear function of permeabilities, increases rapidly at 10^{-14} cm^2, becomes greater than the conductive heat flux function at 10^{-13} cm^2, then increases at a decreasing rate through P3 such that as permeability becomes infinite the heat flux becomes constant, as required by free convection in a single phase system (fig. 7).

Isotherms in P3 are more convex upward than in P1 and P2 and are displaced closer to the surface and inward toward the side contacts at comparable cooling times. This suggests that the distribution of temperature diagnostic mineral assemblages and fluid inclusions around the side contacts of plutons are useful in ascertaining the relative magnitude

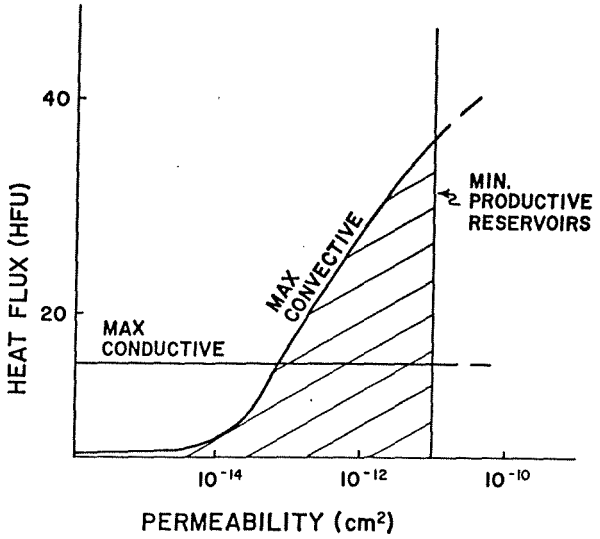

Fig. 7. Maximum vertical heat fluxes calculated at top of pluton as a function of host rock permeability, showing maximum model values for convection and conduction. At point k = 10^{-14} cm² convective heat flux is approximately 10 percent of total heat flux. The minimum permeability at which geothermal fluids are produced is represented by the vertical line at k = 10^{-11} cm² or about 1 millidarcy permeability.

of convective and conductive heat fluxes. At elapsed time = 1.6×10^5 yrs, the 200°C isotherm is shifted toward the pluton with respect to P1. The relatively large vertical heat flux transports thermal energy to the top boundary faster than it can be dispersed through the conductive but impermeable surface, and horizontal fluxes associated with the upward migrating circulation cells produce a plumose pattern in the isotherms (right half of 4C and D). As a result, regions of uniform temperature much broader than the thermal source are produced.

Temperatures in the P3 pluton decrease in a similar manner to the P1 and P2 plutons, since they are cooling essentially by conduction, (figs. 8A and 3); however, the rate of temperature decrease in P3 is greater as a result of increased heat transfer away from the boundaries caused by fluid circulation. Temperature variations with time in the overlying host rocks are complex (fig. 8A), especially when compared to P1 (fig. 3). This complexity is apparently a manifestation of the transport properties of the circulating fluid, the relative rate of conductive and convective heat flux, and numerical effects. The first temperature maxima at t = 4×10^5 yrs occurs in response to convection along the pluton margins and conduction from the pluton. This maxima is analogous to the maxima in P1, except it occurs at smaller elapsed time and is greater in magnitude. The temperature in both systems gradually decreases after this maxima (fig. 3); however, in P3 the temperature increases to a second maxima. These temperature fluctuations with time may be caused by the fluid transport properties. As the fluid column

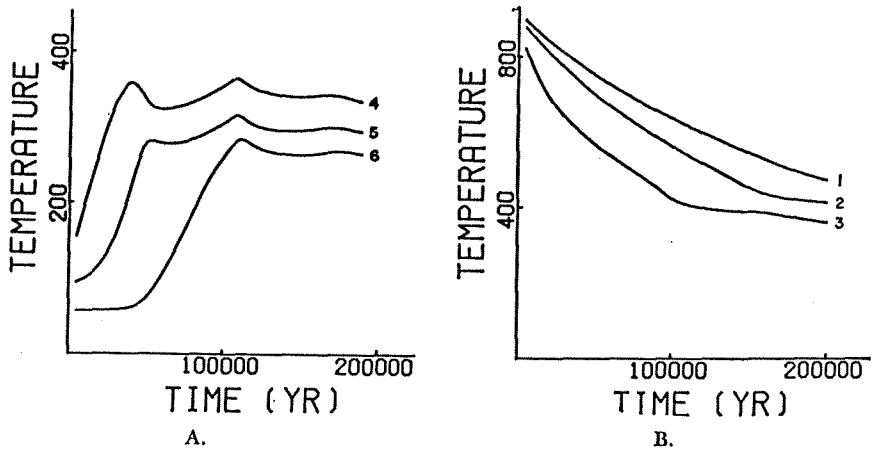

Fig. 8. Temperature as a function of time in system P3 at positions (A) 4, 5, and 6, above top of pluton, 0.45, 1.3, and 3.2 km, respectively, and (B) 1, 2, and 3, below top of pluton, 3.2, 2.3, and 0.45 km, respectively.

above point 4 is heated, fluid density decreases, and, consequently, pressure decreases. Viscosity, thermal coefficient of expansion, and heat capacity of the fluid, therefore, increase, but alpha increases more rapidly than viscosity or heat capacity (paths A and B, fig. 9).

Supercritical-fluid phase properties near the H_2O–system critical end point are continuous and show coincidence of C_p and α maxima and near coincidence of the viscosity minimum in the fluid properties.[3] This maximizes the heat flux at temperatures between 350° to 550°C (fig. 10). Over this temperature range bouyancy forces and heat transport properties are maximized, and the viscous drag force is minimized. Therefore, as conditions in a hydrothermal system cross the extrema in fluid properties from low to high temperature or from high to low pressure, the fluid's heat transport capability first increases then decreases. Therefore, small fluctuations in pressure and temperature may produce large variations in transport properties and cause multiple thermal pulses. Furthermore, in systems whose temperature and pressure conditions do intersect the two-phase surface, the broad oscillations in the temperature-time plot become sharp discontinuities. However, the numerical approximation of the differential equations has contributed an unknown amount to this phenomena. Clearly, the finite difference approximation of alpha across its maxima requires small differential pressure and temperature values. Therefore, we feel that the overall nature of the temperature time plots is realistic but that smaller time period oscillations may be numerical artifacts.

Broad aspects of the temperature-pressure variations in the system define some physical constraints on the development of a two-phase,

[3] The analogous feature is realized in NaCl–H_2O systems, only it is shifted to higher temperatures and pressures because of the corresponding shift in the critical end point.

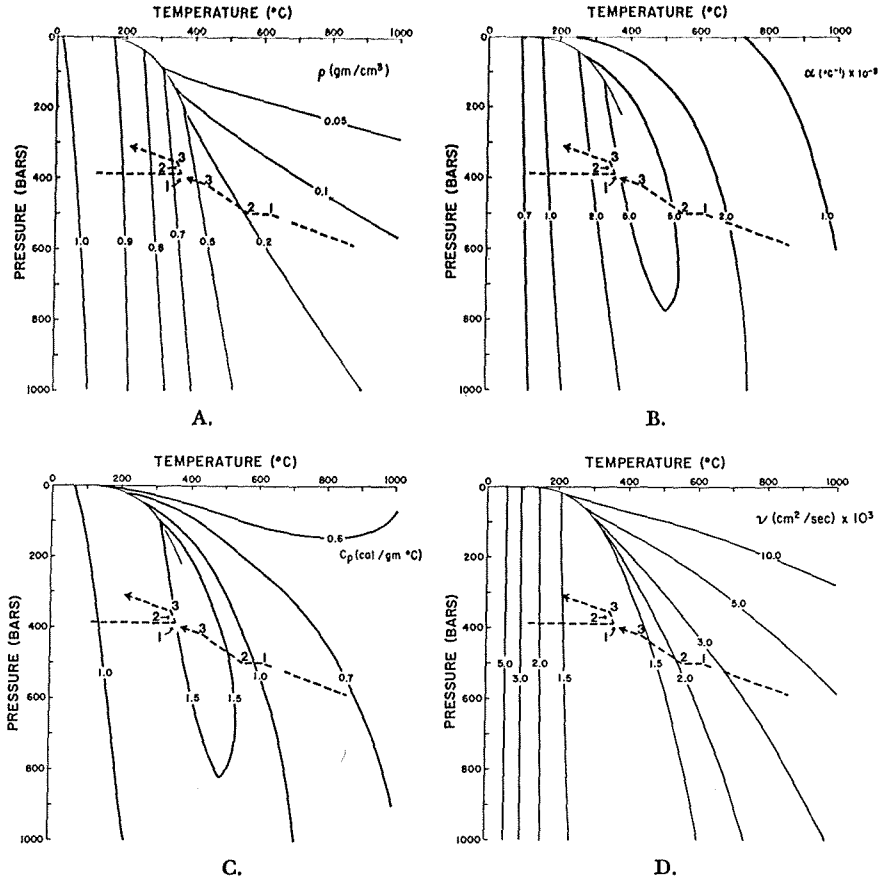

Fig. 9. Temperature-pressure projections of liquid-vapor surface and transport properties of phases in H_2O–system depicting transient temperature and pressure conditions at a position in host rocks 0.45 km above P3 pluton, left dashed line, and 0.45 km below pluton top, right dashed line. Numbers on the dashed lines correspond to maxima on the temperature versus time plot at position 4 in figure 8A. Temperature-pressure variations are shown relative to transport properties: (A) density, ρ, (B) isobaric thermal coefficient of expansion, α, (C) heat capacity at constant pressure, C_p, and (D) viscosity, ν.

liquid-vapor, region. Plutons that are emplaced at depths where the confining pressure is greater than the critical end point pressure do not develop a two-phase system by simple upward transfer of heat. This is evident if we examine the derivative fluid properties along the maximum, for example, for α and C_p, from 1 kb and 450°C to the critical end point (fig. 10). Both α and C_p increase, thereby increasing the transport capability of the fluid and preventing the system's conditions from reaching the two-phase surface.

Stratified.—Plutons emplaced into the upper 10 km of the crust often intrude stratified rocks. Volcanic or sedimentary rock sequences inevitably

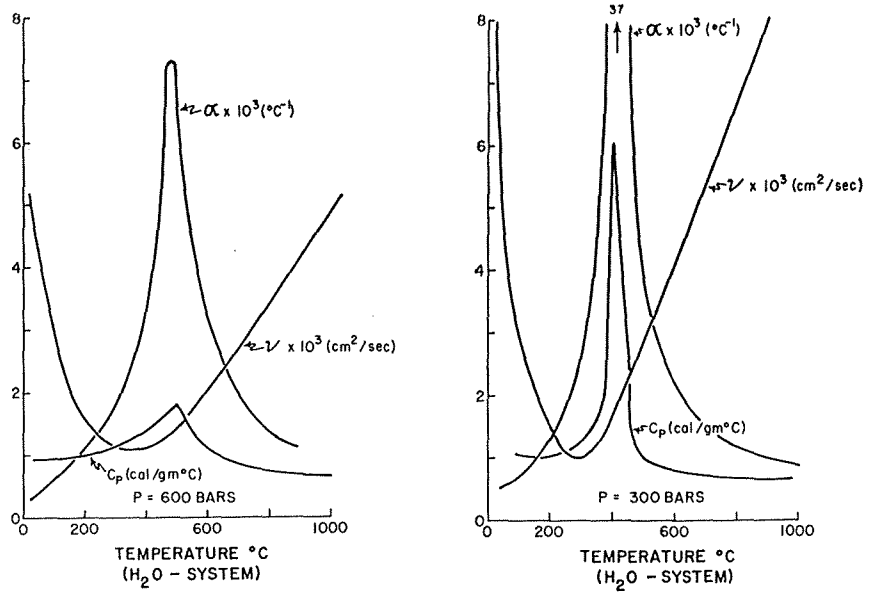

Fig. 10. Thermodynamic and transport properties of supercritical fluid in the H_2O system. The variation of the isobaric coefficient of thermal expansion, α, isobaric heat capacity, C_p, and viscosity, ν, with temperature at (A) 600 bars and (B) 300 bars pressure.

have vertical variations in permeability that may affect the style of fluid circulation and, consequently, the pluton's cooling history. This type of system is simulated by P4, which consists of a pluton intruded into a layered stratigraphic sequence (fig. 11).

Stratified rocks confine fluid circulation to the more permeable layers (fig. 12). Streamlines are refracted at permeability discontinuities, but since the streamlines are developed into circular like cells, the refraction often does not appear to coincide with the actual physical

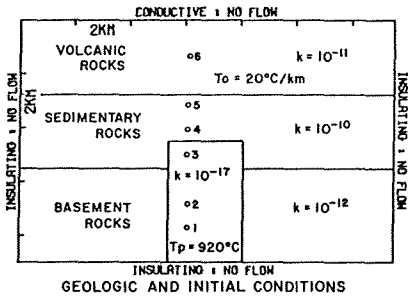

Fig. 11. Two-dimensional cross section of a pluton, P4, and stratified host rocks. Boundary conditions and (left) geologic conditions are depicted for an impermeable pluton emplaced at 920°C; (right) initial conditions depicted for a temperature of 20°C at the top boundary and a thermal gradient of 20°C/km. Constant permeability was maintained in the host rocks, but stepwise permeability increases were included for the upper portion of the pluton in order to simulate fracturing. The domain was represented by 160 grid points at regular intervals, $\Delta z = 0.9$ km and $\Delta y = 1.35$ km.

boundary. This style of fluid circulation accentuates the displacement of isotherms toward the sides of the pluton (right half of 12D; right half of 13A). The plumose outline of isotherms noted in P3 is not as well developed in P4, nor do the isotherms reach as near to the surface. The thermal energy dispersed laterally into the permeable unit is redispersed by conduction and results in a very broad doming of the isotherms in the upper portion of the system (see 100°C, right half of fig. 12A).

Time.—The effective stresses associated with the emplacement of magmas, their crystallization, and concomitant heating of the surrounding host rocks produce systematic and relatively abundant fractures in plutons and host rocks. Although the distribution of fracturing in time is poorly known, the crosscutting relationships observed in natural systems suggest a complex sequence of fracturing events. Crystallization of fluid bearing magmas may release substantial mechanical energy; therefore, the P4 pluton's permeability was increased early in its cooling history to simulate fracturing. Permeability variations were chosen arbitrarily, but the time of fracturing was chosen when the temperature decreased to $\sim$ 860°C. Fracturing was approximated by an instantaneous increase in permeability.

The upper 0.9 km portion of the pluton was fractured at t = 1250 yrs, and permeability was increased to 10^{-11} cm^2 (left half of fig. 13A).

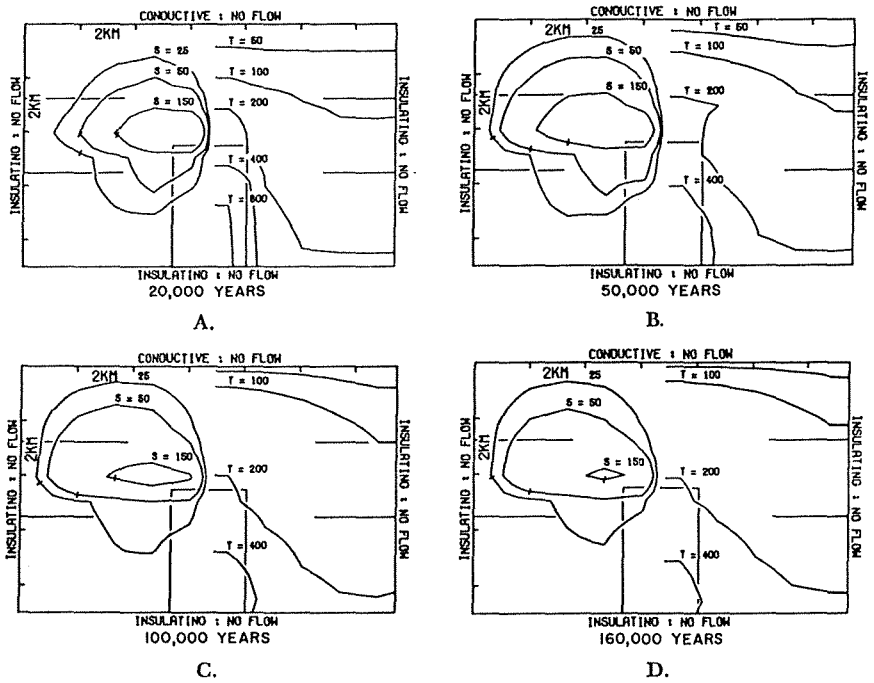

Fig. 12. Steady state (left) dimensionless streamfunction and (right) temperature distribution in system P4. Horizontal broken lines depict stratified permeability boundaries, (A) at 2×10^4 yrs, (B) at 5×10^4 yrs, (C) at 10^5 yrs, (D) at 1.6×10^5 yrs.

Comparison of the pre-fracture fluid circulation at t = 1200 yrs (left half of fig. 13B) with the post-fracture pattern at t = 2000 (left half of fig. 13C) illustrates both the deeper penetration of flow into the pluton and increasing fluid fluxes (table 2). A second fracture event at t = 5000 yrs (right half of fig. 13D) increased permeability to 10^{-10} cm^2 in the upper 0.9 km of the pluton and to 10^{-12} cm^2 in the next lower 1.8 km. Again the fluid circulation at t = 5×10^3 yrs (left half of fig. 13D) and at t = 2×10^4 yrs (left half of fig. 12A) illustrates the effect of the permeability increase.

The two increases in pluton permeability over 5×10^3 yrs have a dramatic effect on the fluid flux and thermal decay of the pluton (fig. 14). Specifically, the upper 0.9 km of the pluton cools at 0.12°C/yr for 5000 yrs, and the next lower 1 km cools at 0.02°C/yrs for 17500 yrs; thereafter temperature decreases at 10^{-4}°C/yr in both regions. Consequently, the temperature in the upper 2 km averages 260°C for 2×10^5 yrs. The coincidence of emplacement into shallow portions of the crust and thorough fracturing of the pluton rapidly cools the entire body to temperatures between 200° to 400°C.

Increased permeability increases fluxes in both the vertical and horizontal directions such that the thermal energy is more quickly dispersed.

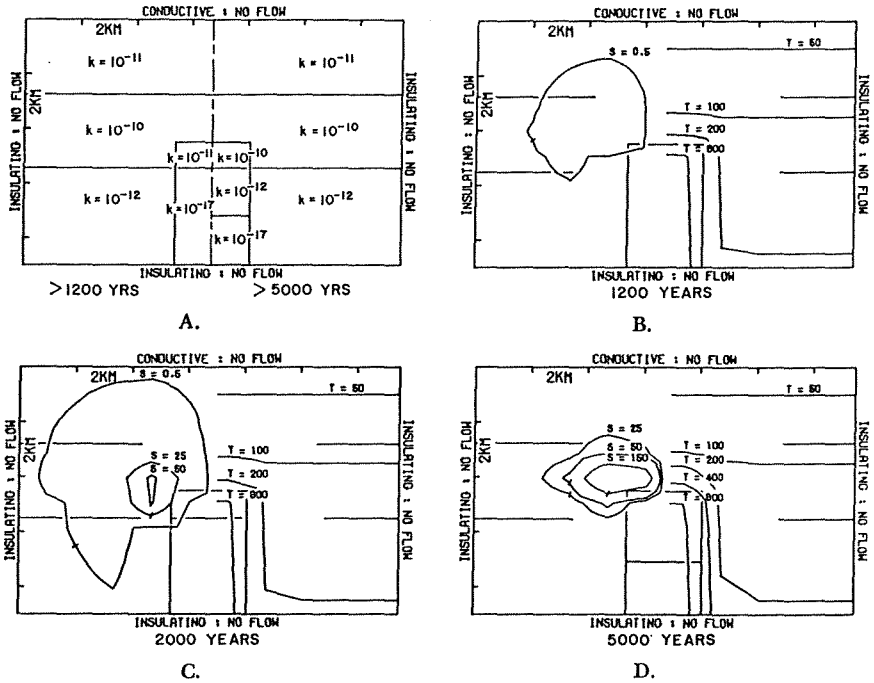

Fig. 13. Thermal history of P4 during short elapsed times when pluton permeability was increased to simulate fracturing. (A) Permeability distribution in systems (left) 1200 yrs < t < 5000 yrs (right). (B–D) Steady state (left) dimensionless streamfunction and (right) temperature distribution in system P4. Horizontal broken lines in host rocks and horizontal solid lines in pluton depict stratified permeability boundaries at (B) 1200 yrs, (C) 2000 yrs, (D) 5000 yrs.

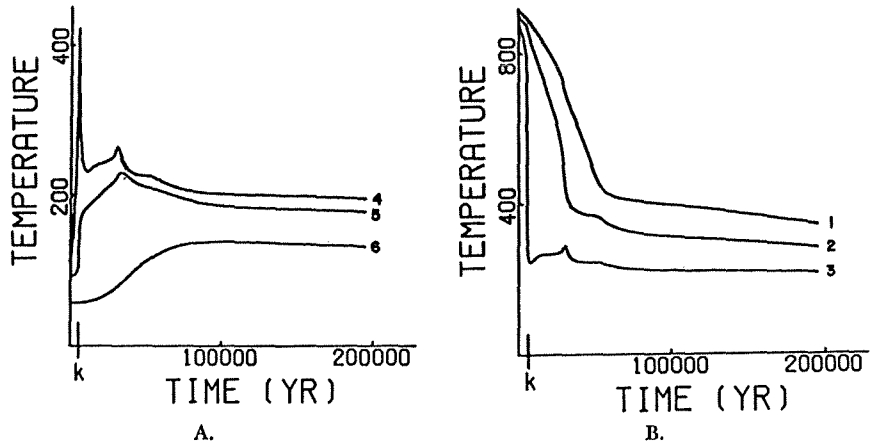

Fig. 14. Temperature as a function of time in system P4 at fixed points (A) 4, 5, and 6, above top of pluton, 0.45, 1.3, and 3.2 km, respectively, and (B) 1, 2, and 3, below top of pluton, 3.2, 2.3, and 0.45 km, respectively. Symbol k denotes approximate times at which pluton permeability was increased in order to simulate fracturing.

However, the thermal history at a position 4 km above the pluton does not reveal evidence of the pluton fracturing.

Fracture zone.—Conditions where igneous activity is most common are conducive to the formation of numerous fractures, both within the pluton and in host rocks. The effects of fracture controlled permeability within host rocks over the top of the pluton were analyzed using model P5 (fig. 15A).

Fluid circulation is confined to the permeable zone above the pluton. The streamline pattern also differs from previous models, because the system boundaries are open to fluid flow (figs. 15B–D). Circulation cells, centered within the fracture zone, reduce the broad isotherm surface observed in previous systems to a much narrower and larger amplitude surface confined to the fracture zone. The broader low amplitude doming of the isotherms is primarily the result of conduction heat away from the fracture zone (right half of fig. 15D). Temperature variation with time within the pluton follows a normal conductive cooling pattern, except that the upper 1 km of the pluton is cooled at an increased rate by fluid circulation.

Temperatures within the fracture zone are similar in distribution but lower in magnitude than previous systems: Lower values of temperature, relative to model P3, are a result of the narrow, large permeability fracture zone and the height of the thermal anomaly in the fracture zone (figs. 16 and 8). However, the temperature-time curves are quite similar in magnitude to P4 (fig. 14), illustrating the common effect of increased permeability.

Pluton geometry.—The vertical extent of the pluton exposed to permeable host rocks determines the lateral extent of the fluid circulation. This effect was simulated by model P6, where the vertical exposure of the pluton was decreased to 2.7 km by introducing a layer of 10^{-17}

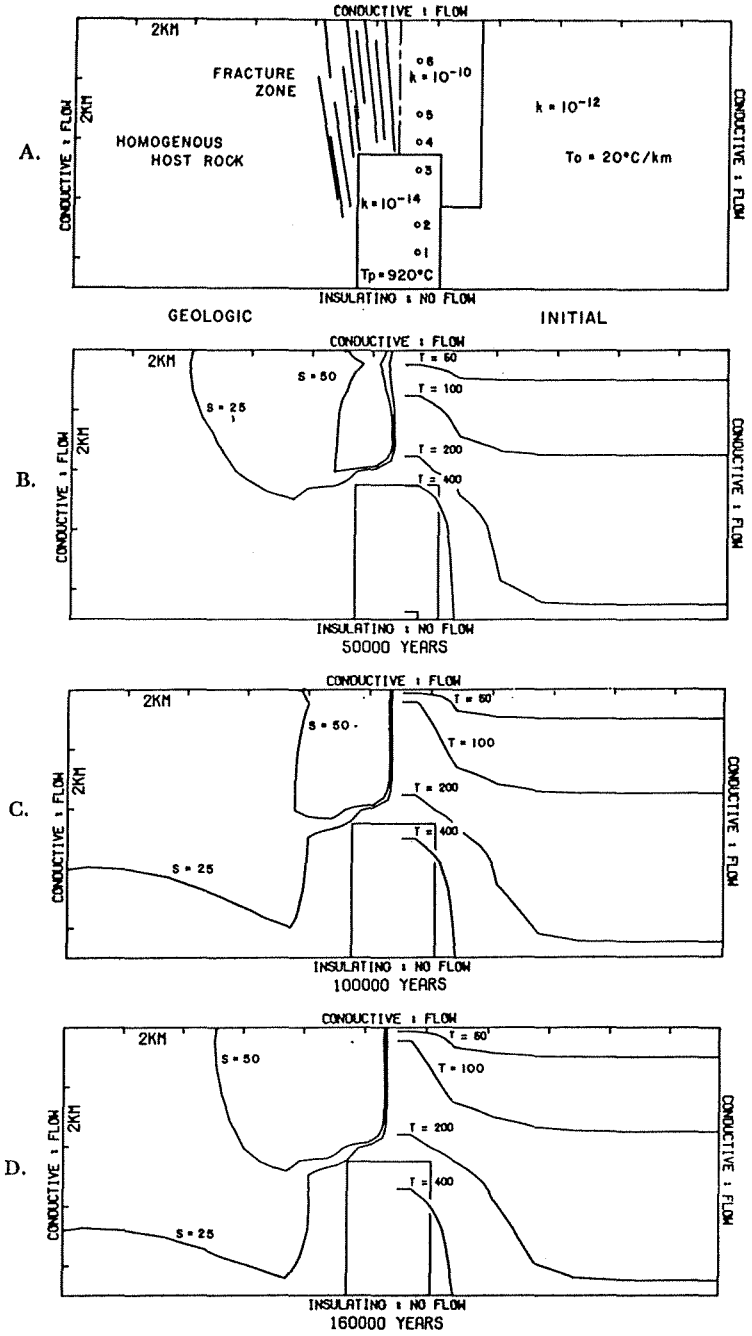

Fig. 15. Two-dimensional cross section of system P5 depicting boundary conditions and (A) initial (left) and geologic (right) conditions for anomalously high permeability zones directly over the top of pluton. Pluton is emplaced at 920°C into host rocks whose temperatures are defined by 20°C top boundary temperature and a 20°C/km thermal gradient. The domain was represented by 160 grid points at regular intervals, $\Delta z = 0.9$ km and $\Delta y = 1.35$ km. (B–D) Steady state (left) dimensionless streamfunction at (B) 5×10^4 yrs, (C) 10^5 yrs, (D) 1.6×10^5 yrs; (right) temperature distribution at (B) 5×10^4 yrs, (C) 10^5 yrs, (D) 1.6×10^5 yrs.

cm^2 permeability across the base of the domain (fig. 17A). In the upper portion of the system heat is transferred away from the pluton by convection. Fluid circulation is centered over the side contact and 1 km above the top of the pluton at 5×10^5 yrs and migrates upward 1 km by $t = 1.6 \times 10^5$ yrs (fig. 17, B–D). However, in P3, fluid circulation is centered in the host rocks laterally away from the side contact, as well as above the top contact (fig. 4, B–D). The height of the circulation cells is less in P6 than in P3, and the lateral extent of the cells is also proportionately smaller. The ratio of the cell widths is approximately equal to the ratio of the effective pluton heights for the two systems. Therefore, plutons with the larger effective heights will cause fluid circulation a greater distance from their side contacts.

The convective heat flux at $t = 2 \times 10^4$ yrs is equivalent over the plutons in both P3 and P6, but P6 has 10 percent greater flux along its side margins (figs. 6A and 18). This difference increases to 50 percent between 5×10^4 yrs and 10^5 yrs, then decreases to 45 percent at 1.6×10^5 yrs (fig. 19). These differences between the two systems are also evident in the temperature variations with time, although the initial temperature increase above the pluton tops is nearly identical, figures 20 and 8. The second inflection point in each of the temperature-time curves is shifted to earlier times and is of lower magnitude for the shorter pluton.

Level.—Plutons emplaced at levels < 2.2 km generate initial conditions that include two-phase fluid flow with respect to H_2O–systems; those emplaced at increasing depth greater than 2.2 km generate thermal anomalies that are proportionately more extended in the vertical direction. The theory and numerical equations used in this study do not afford for two-phase flow; therefore, the effect of pluton emplacement at depths greater than 2.2 km was examined. The effective height of pluton P7 in permeable rocks is 2.7 km, equivalent to P6, but P7 is 6.3 km deep (left half of fig. 21A).

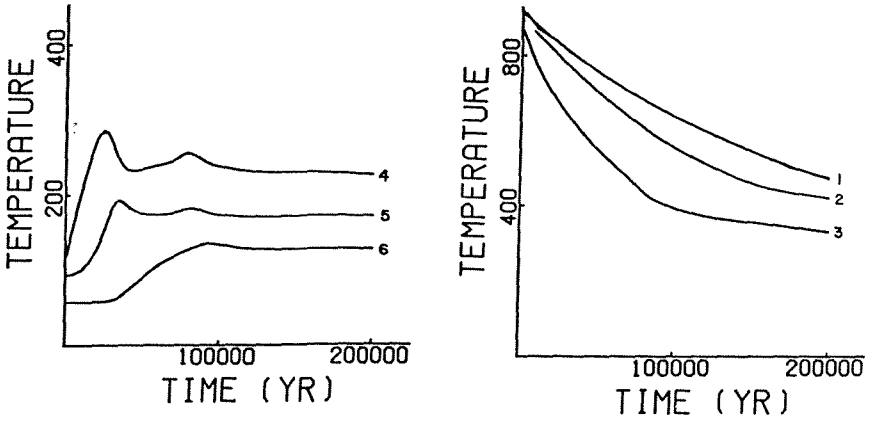

Fig. 16. Temperature as a function of time in system P5 at fixed positions (A) 4, 5, and 6, above top of pluton, 0.45, 1.3, and 3.2 km, respectively, and (B) 1, 2, and 3, below top of pluton, 3.2, 2.3, and 0.45 km, respectively.

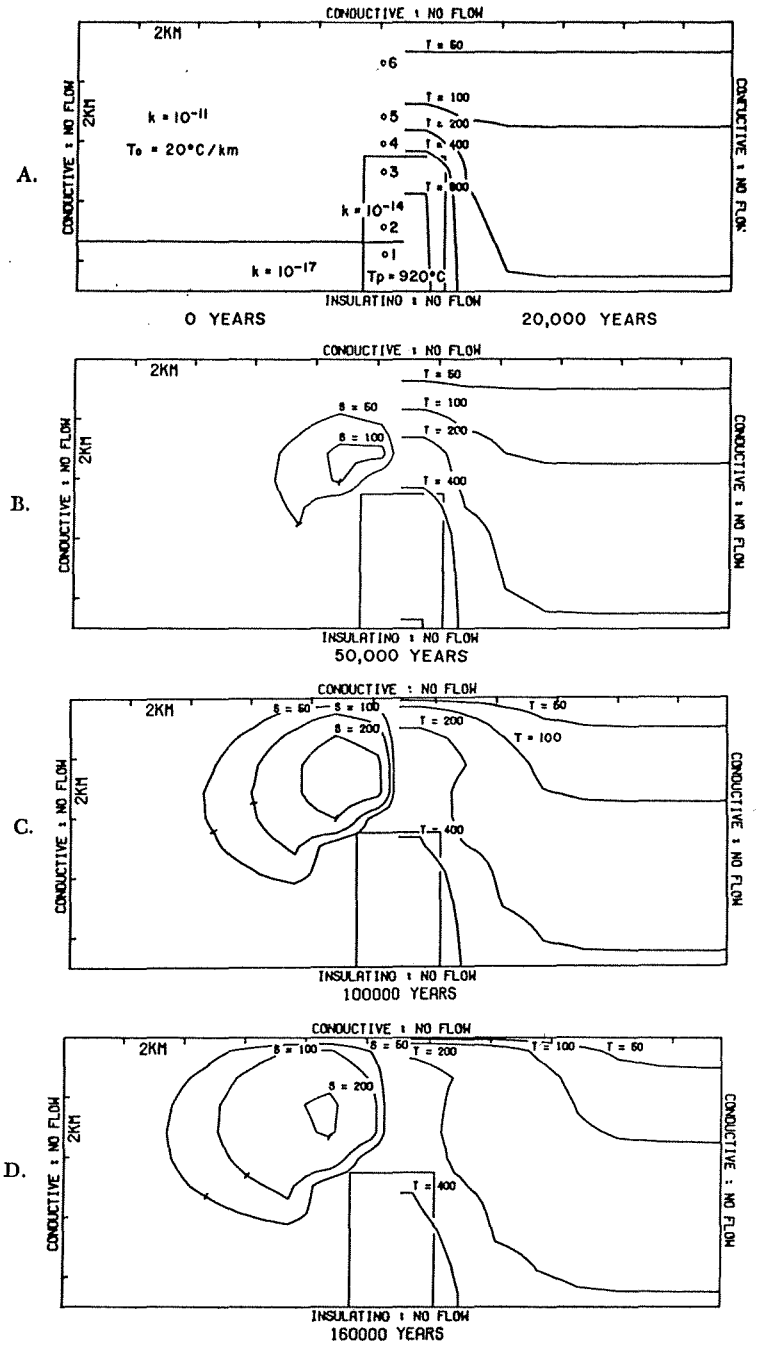

Fig. 17. Two-dimensional cross section of system P6 depicting boundary conditions and (left): (A) initial conditions for pluton identical to P3 except for low permeability layer at base of system. (B–D) Steady state dimensionless streamfunction at (B) 5×10^4 yrs, (C) 10^5 yrs, (D) 1.6×10^5 yrs; (right) temperature distribution at (A) 2×10^4 yrs, (B) 5×10^4 yrs, (C) 10^5 yrs, (D) 1.6×10^5 yrs.

Fluid circulation is similar initially around plutons P7 and P6 since the thermal perturbation with respect to the surroundings is similar (left half of fig. 21B). However, as the thermal anomaly from P7 becomes dispersed over the 6.3 km between the top of the pluton and the surface, larger circulation cells develop (left half of fig. 17D and left half of fig. 21D). This extension of the anomaly results in a plumose isotherm pattern similar to the taller and shallower pluton in P3 but is less extensive in width and height because of the lower total energy content of the P7 pluton (right half of figs. 21C, 21D, and 4D).

Width.—A batholith size pluton was simulated with model P8 (fig. 23). Fluid circulation in P8 is similar to other systems but is upward along the side contacts of the relatively impermeable pluton around the top corner and upward from the top contact (left half of figs. 23D–F).

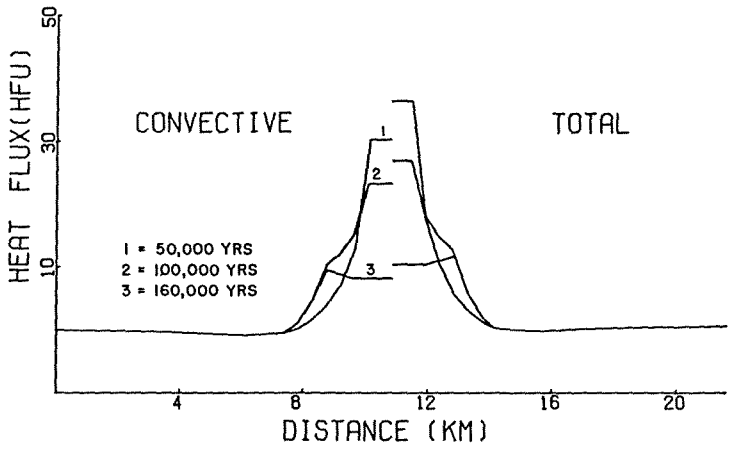

Fig. 18. Vertical component of convective and total heat fluxes as a function of distance along a horizontal plane coincident with the top of P6 pluton at elapsed times of 5×10^4 yrs, 10^5 yrs, and 1.6×10^5 yrs.

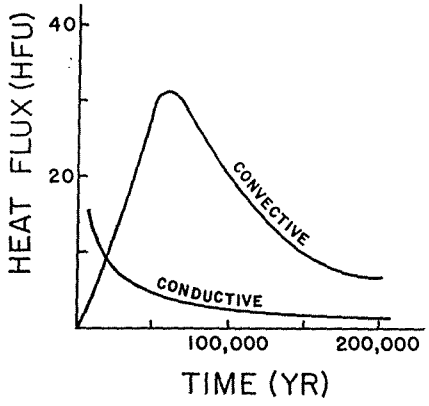

Fig. 19. Maximum convective and conductive heat fluxes as a function of time at top of P6 pluton.

This flow style eventually generates a secondary thermal perturbation due to the width of the pluton (right half of fig. 23F). The effect of the pluton width is to delay the development of fluid circulation over the top of the batholith. Therefore, upward displacement of isotherms is less over the pluton top than at its sides (right half of figs. 23D–F). This lateral temperature perturbation produces secondary circulation cells. These circulation cells further accentuate the temperature anomaly by depressing the isotherms in the central downflow zone (right half of fig. 23F). The secondary cells eventually dominate over the fluid circulation along the side contacts (left half of fig. 23F), and circulation breaks up into 4 Bénard-like cells (Bénard, 1901). As a consequence of this circulation pattern, a 60 km^2 region over the top of the batholith remains at 400°C for 10^6 yrs.

Undoubtedly, the perfectly flat top pluton which extends for 54 km is geologically unreasonable. However, it does indicate an extreme condition which, together with the stock sized plutons in previous models, can be used to analyze the nature of heat transport from a batholith sized body which may have stocks protruding from its upper boundary or for a broad convex topped batholith. Batholiths with convex tops tend to decrease the tendency for secondary cells to develop. Irregular topography, consisting of apical stocks on the batholith top, will develop secondary convective cells around each topographic feature.

Relative cooling rates.—Differences in the cooling rates are insignificant for systems for which pluton size and permeability are equal (table 3). Although large fluid flux occurs along the margins of systems P3 and P6, this does not increase the cooling rate of the pluton significantly. Fluid circulation has its greatest effect in redistributing the thermal energy upward toward the surface as opposed to laterally away from the

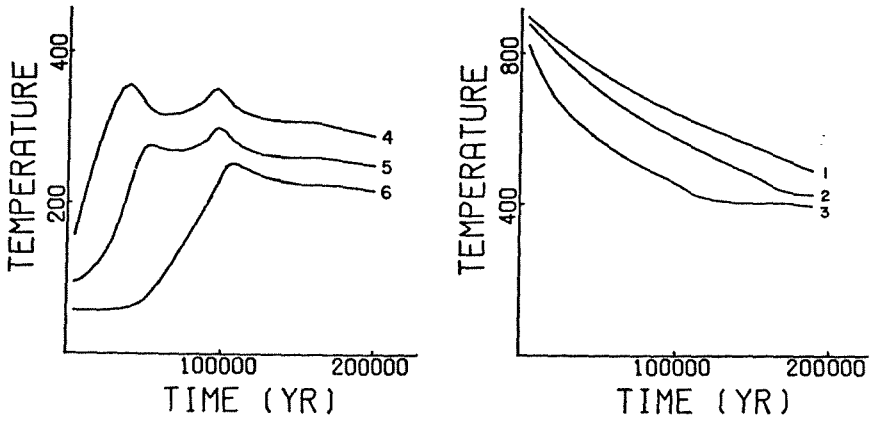

Fig. 20. Temperature as a function of time in system P6 at fixed positions (A) 4, 5, and 6, above top of pluton, 0.45, 1.3, and 3.2 km, respectively, and (B) 1, 2, and 3, below top of pluton, 3.2, 2.3, and 0.45 km, respectively.

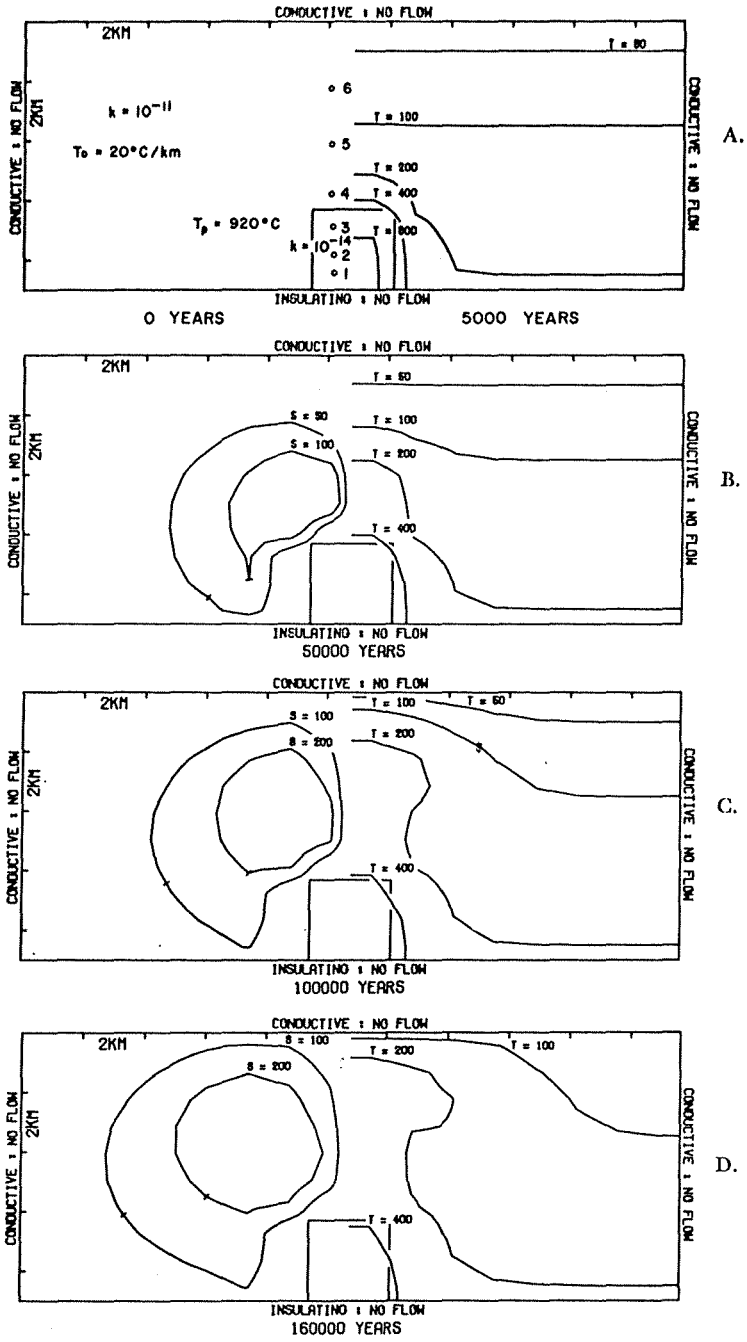

Fig. 21. Two-dimensional cross section of system P7 depicting boundary conditions and (A) initial conditions (left) for a 2.7 km tall pluton emplaced at 920°C into uniform permeability host rocks. Host rock temperature and permeability are same as system P3. The domain was represented by 160 grid points, $\Delta z = 0.9$ km and $\Delta y = 1.35$ km. (B–D) Steady state (left) dimensionless streamfunction at (B) 5×10^4 yrs, (C) 10^5 yrs, (D) 1.6×10^5 yrs; (right) temperature distribution at (A) 5×10^3 yrs, (B) 5×10^4 yrs, (C) 10^5 yrs, (D) 1.6×10^5 yrs.

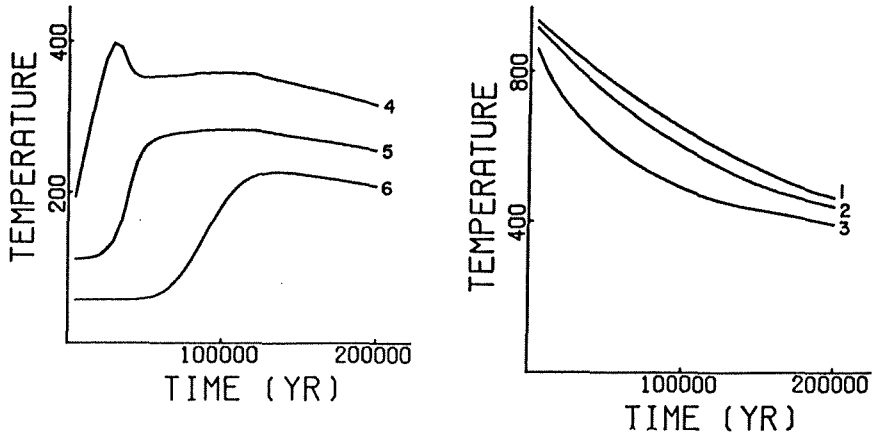

A. B.

Fig. 22. Temperature as a function of time in system P7 at fixed points (A) 4, 5, and 6, above top of pluton, 0.45, 1.3, and 3.2 km, respectively, and (B) 1, 2, and 3, below top of pluton, 3.2, 2.3, and 0.45 km, respectively.

pluton. Plutons with permeabilities 10^{-14} cm^2 tend to cool much more rapidly than their relatively impermeable counterparts, compare P4 with P3.

Fluid redistribution.—The redistribution of large quantities of fluid is a direct consequence of fluid circulation in pluton environments. This redistribution and concomitant changes in temperature and pressure give rise to an overall irreversible chemical interaction between fluids and minerals. The purpose of this section is to examine some of the features of fluid redistribution in model systems.

Fluid circulation is represented by the distribution of streamlines in each of the systems; however, of more direct interest to mass transport computations is the actual distance and path along which a given fluid packet moves during the thermal event. These fluid pathlines, as defined by eq (36), are analogous to a time exposure of a single fluid packet as it circulates through the system. Pathlines for fluid packets whose origins are in various portions of a system are dependent on the rock permeability and proximity of the path origin to the thermal anomaly (figs. 24, 26, 28, 30, and 32). Fluids initially in the upper portions of low permea-

TABLE 3

Pluton cooling rates

System	Fraction of initial anomaly after 2×10^5 yrs	
P1	0.4	conduction
P3	0.4	convection in host rocks
P4	0.2	permeable pluton
P5	0.4	fracture zone in host rocks
P6	0.4	less exposed in impermeable rocks
P7	0.3	shorter and deeper pluton
P8	0.8*	batholith

* 0.45 after 1.2×10^6 yrs

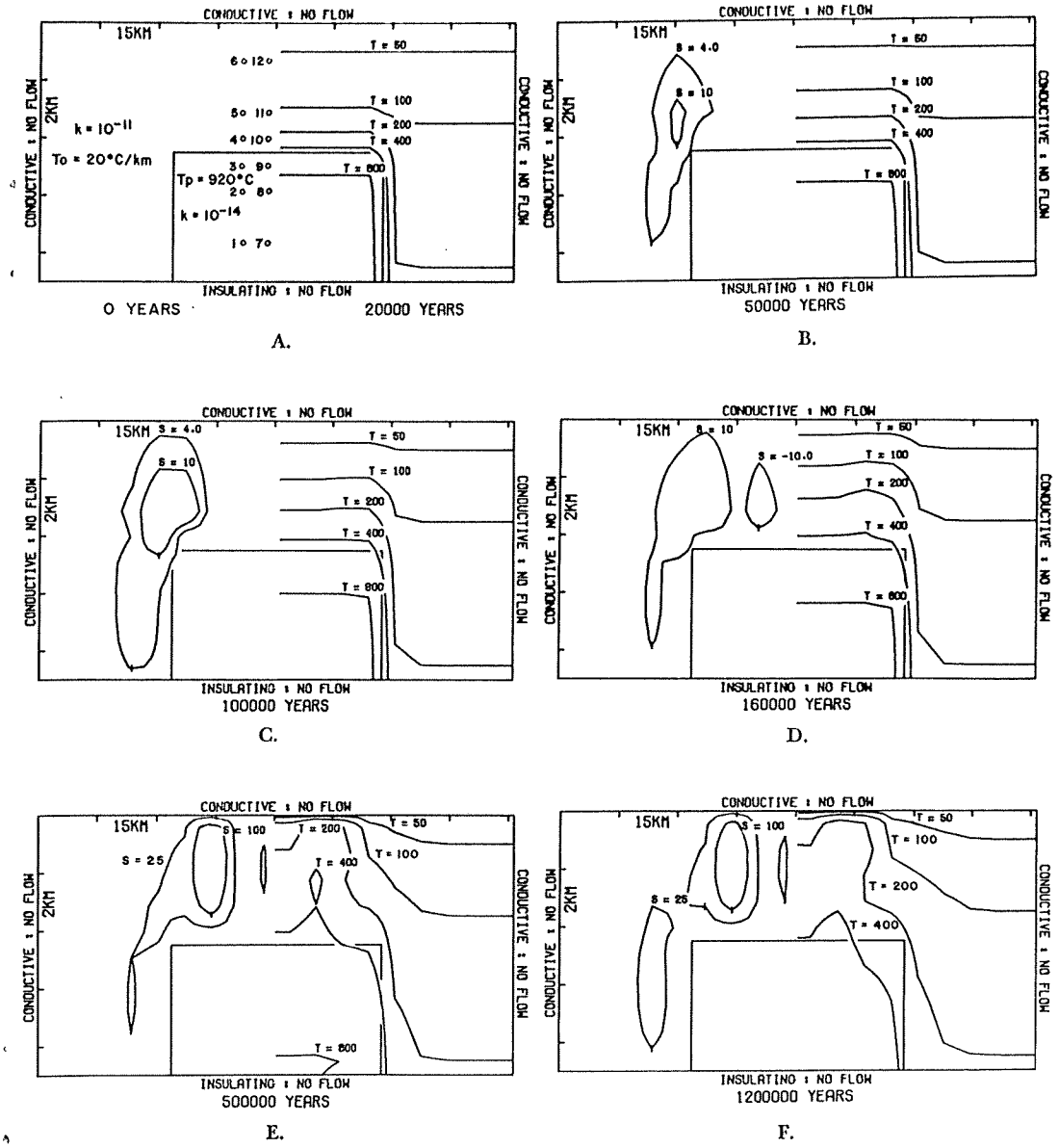

Fig. 23. Two-dimensional cross section of system P8 depicting boundary conditions and (A) initial conditions (left) for batholith size intrusive emplaced into domain with conditions similar to P3. The domain is represented by 180 grid points, $\Delta z = 0.9$ km and $\Delta y = 6.75$ km. (B–D) Steady state (left) dimensionless streamfunction at (B) 5×10^4 yrs, (C) 10^5 yrs, (D) 1.6×10^5 yrs, (E) 5×10^5 yrs, (F) 1.2×10^6 yrs; (right) temperature distribution at (A) 2×10^4 yrs, (B) 5×10^4 yrs, (C) 10^5 yrs, (D) 1.6×10^5 yrs, (E) 5×10^5 yrs, (F) 1.2×10^6 yrs.

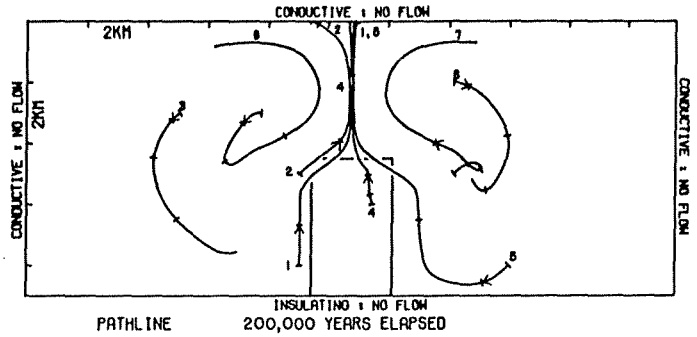

Fig. 24. Examples of fluid pathline in system P3 representing the redistribution of fluids caused by the thermal anomaly. Arrows indicate direction of fluid motion; tic marks occur every 5×10^4 yrs.

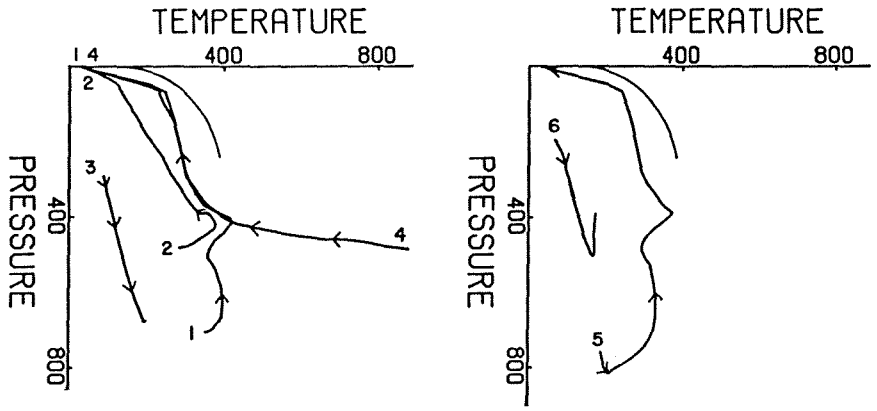

Fig. 25. Pressure-temperature path of fluid packets that circulate along paths in system P3 (fig. 24). Paths are shown with respect to liquid-vapor surface in H_2O system.

bility plutons flow relatively short distances in the initial 10^5 yrs (for example, 1 km in systems P3, P5–P7, figs. 24, 28, 30, and 32). During the subsequent 10^5 yrs fluid circulation increases enough in the upper portions of the pluton to transport fluid packets several km into the overlying host rocks. Fluids initially in larger permeability plutons are transported completely out of the pluton in the initial 10^5 yrs (fig. 26). As a result, this fluid is replaced by fluid packets circulating along pathlines into the sides of the pluton.

Fluids initially in host rocks several km away from the pluton convect toward and into the pluton (fig. 24). The pathlines trend along the side contacts of low permeability plutons, whereas they flow into the plutons with larger permeability (fig. 26). As the fluids move horizontally toward the pluton, the circulation center migrates upward in the system. Therefore, pathlines with origins above the pluton tend to form upward looping spirals. Stratified permeabilities restrict pathline movement to

the larger permeability units. In P4 layered units force the circulation toward the pluton (fig. 26), and, since P4 is a relatively permeable pluton, fluid packets then circulate through the pluton.

Fracture zones effectively channel the fluid up through the fracture zone. Pathlines in the vertical fracture zone are proportionately longer than those in the adjacent, less permeable rocks (fig. 28). Transit time for these packets from the top of the pluton to the surface is 10^5 yrs.

Changes in temperature and pressure along fluid pathlines describe a path through the H_2O system along which the solvent properties of the fluid may be described and define the intensive variables required to calculate mass transfer between fluid and rock. Packets of supercritical fluid, whose temperatures are in the critical endpoint region, are subjected to drastic changes in thermodynamic and electrostatic properties (figs. 25, 27, 29, 31, and 33). Extreme variations in thermodynamic behavior of the solvent along these paths are apparent from the work by Helgeson and Kirkham (1974a,b).

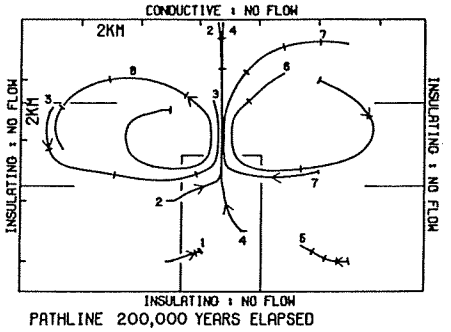

Fig. 26. Examples of fluid pathline in system P4 representing the redistribution of fluids caused by the thermal anomaly. Arrows indicate direction of fluid motion; tic marks occur every 5×10^4 yrs.

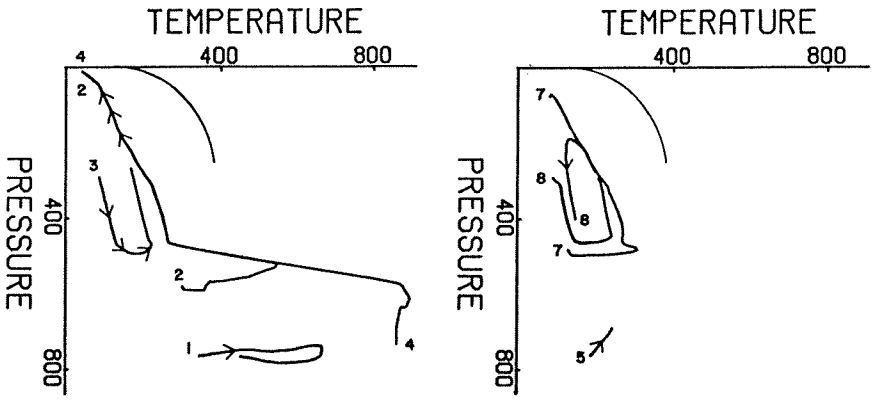

Fig. 27. Pressure-temperature path of fluid packets that circulate along paths in system P4 (fig. 26). Paths are shown with respect to liquid-vapor surface in H_2O system.

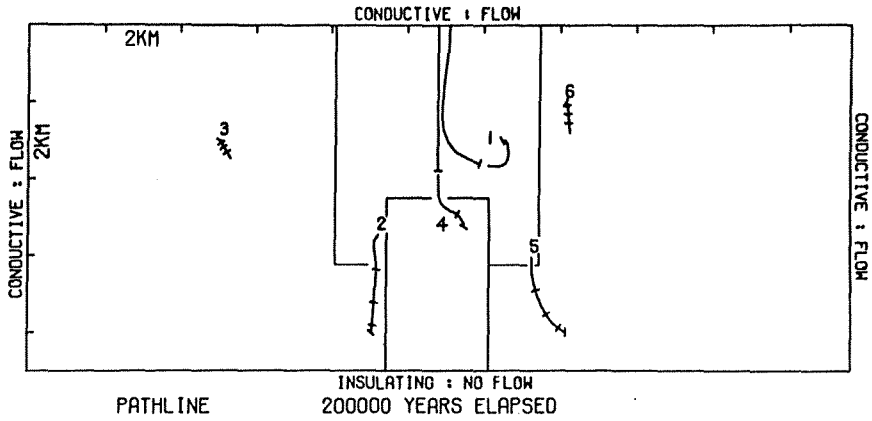

Fig. 28. Examples of fluid pathline in system P5 representing the redistribution of fluids caused by the thermal anomaly. Arrows indicate direction of fluid motion; tic marks occur every 5×10^4 yrs.

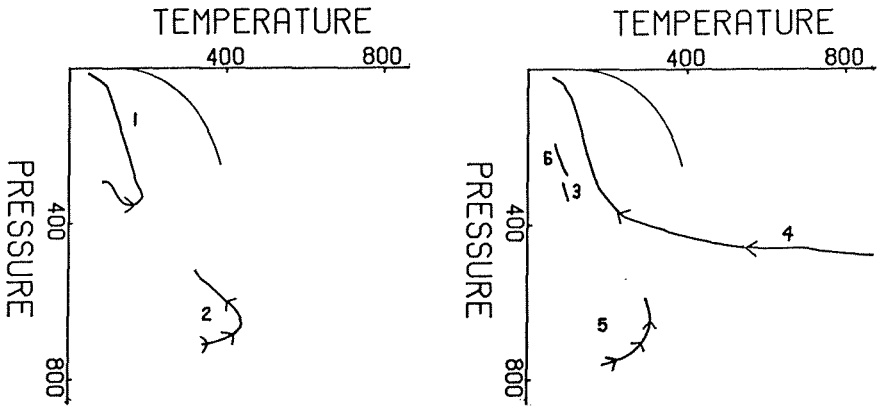

Fig. 29. Pressure-temperature path of fluid packets that circulate along paths in system P5 (fig. 28). Paths are shown with respect to liquid-vapor surface in H_2O system.

Enormous quantities of fluid are circulated through pluton environments where thermal convection is the predominant cooling process. The total mass of fluid circulating through a unit area, integrated over a time interval of 2×10^5 yrs for each system (table 4), is considerably less for low permeability plutons than for the fractured plutons.

The mass of fluid that flows during time interval t_2–t_1, through an area, A, normal to a fluid pathline is defined by

$$M_f = A \int_{t_1}^{t_2} \rho_f \bar{v} dt, \tag{58}$$

where $\bar{v}$ is the Darcy velocity and ρ_f is the density of the fluid. The mass

of rock exposed to the circulating mass of fluid is defined in terms of the true velocity, $\bar{v}_t$, of the fluid:

$$M_r = A\,(1-\phi)\int_{t_1}^{t_2} \rho_r \bar{v}_t dt, \tag{59}$$

where ϕ is the flow porosity and ρ_r is the density of the rock. The mass ratio of circulating fluid to rock contacted by the fluid is the ratio of eqs (58) and (59), if the average fluid velocity over the time interval is used:

$$\frac{M_f}{M_r} = \frac{\phi}{1-\phi}\,\frac{\int_{t_1}^{t_2} \rho_f dt}{\int_{t_1}^{t_2} \rho_r dt}, \tag{60}$$

since the true velocity is related to the Darcy velocity by

$$\bar{v}_t = \frac{\bar{v}}{\phi}. \tag{61}$$

The rock density is nearly constant over temperature ranges realized in pluton environments, and the fluid density varies from 0.2 to 0.9 g cm^{-3}. Therefore, fluid-rock mass ratios are approximately

$$\frac{M_f}{M_r} \approx \frac{\phi\,\rho_f}{(1-\phi)\,\rho_r}. \tag{62}$$

TABLE 4

Mass of fluid circulated through systems (g cm^{-2} × 10^5)

Position	System P3	P4	P5	P6	P7
1	0.3	0.02	0.3	trace	trace
2	0.5	4	0.4	0.5	0.4
3	0.7	24	0.6	0.5	0.5
4	22	35	20	15	20
5	33	27	30	15	20
6	24	5	20	20	20

TABLE 5

Fluid:rock mass ratios

Position	P3	P4	P5	P6	P7
1	0.05	0.1	0.06	0.07	0.1
2	0.08	0.16	0.1	0.1	0.1
3	0.1	0.3	0.1	0.1	0.1
4	0.25	0.31	0.31	0.26	0.25
5	0.28	0.32	0.33	0.3	0.28
6	0.30	0.33	0.34	0.3	0.30

The effective mass ratio (table 5), defined by eq (60), permits computation of fluid-rock reactions from the viewpoint of a circulating or stagnant fluid. In rocks where the fluid flow is confined to fractures, the flow porosity may be on the order of 10^{-4} to 10^{-5} (Norton and Knapp, 1977), and, therefore, the $(1-\phi)$ term in the denominator is $\cong 1$, and the effective mass ratio is on the order of the flow porosity, since $\rho_r \cong 2.73$ g cm^{-3}. These mass ratios are exceedingly small compared to those predicted from stable light isotope data on hydrothermal systems (Taylor, 1971). The reason for this discrepancy is obvious, since eq (60) defines the mass of rock contacted by a circulating mass of fluid, whereas the isotopic data estimates the integrated effect of all fluid packets circulating through an arbitrary rock mass.

The total mass of fluid that circulates through an arbitrary mass of rock, at a fixed position in a hydrothermal system, is normally used in predicting the amount of isotopic or other chemical exchange that occurs

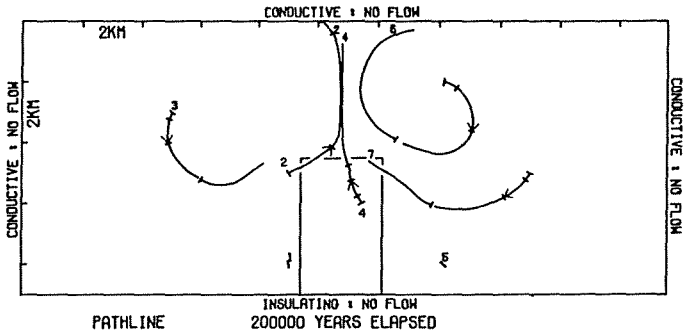

Fig. 30. Examples of fluid pathlines in system P6 representing the redistribution of fluids caused by the thermal anomaly. Arrows indicate direction of fluid motion; tic marks occur every 5×10^4 yrs.

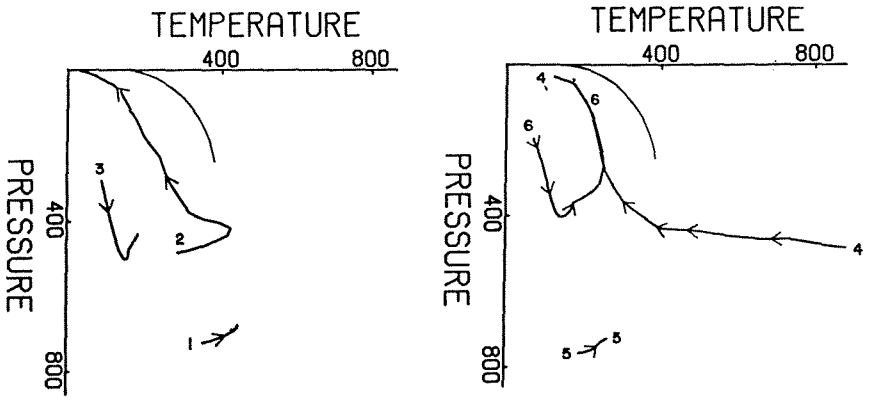

Fig. 31. Pressure-temperature path of fluid packets that circulate along paths in system P6 (fig. 30). Paths are shown with respect to liquid-vapor surface in H_2O system.

This ratio is essentially the integrated amount of fluid passing through the rock. Ratios computed from eq (64) for the model systems range from positive infinity, for infinity thin rock wafers, to values on the order of 0.5 when the rock volume is the entire thermal anomaly. Circulation of reactive fluids through these environments can not be adequately simulated by the numerical equation used for the circulation of inert fluids but requires explicit equations for exchange, reaction, diffusion, and advection of components, as suggested in Norton and Knapp (1977). Simulation of these types of systems will be the topic of a future communication.

CONCLUSIONS

Spatial and temporal variations in fluid flow and heat flux in a sequence of simplified geologic systems indicate that bulk rock permeabilities in host rocks around hot plutons that are $\geq 10^{-14}$ cm^2 result in convection of thermal energy upward along the sides of the pluton and toward the surface. However, only in those systems that contain permeable plutons is the cooling rate increased. The rather small variation in permeability over which the transition from conductive to convective heat transfer occurs and the relatively low threshold value of permeability required for significant convective heat transfer suggest that heat transfer by circulating fluids may be significant over very broad crustal regions where temperature perturbations occur within the crust. Temperature conditions around plutons that cool by convective heat transfer are substantially different from their conductive dominated equivalents. Large volumes of rock above shallow plutons remain at nearly constant temperature for very long periods of time. The temperature is nominally in the range of 200° to 400°C for the upper crust. This feature and the circulation of large masses of fluid from considerable distances away from the thermal anomaly undoubtedly affect the thermal metamorphism and hydrothermal alteration of rocks in the pluton's vicinity.

Heuristic models of hot pluton environments suggest that fluid circulation is an integral part of their cooling process. Major features of the hydrothermal system noted in these models are undoubtedly evident in their natural analogs. Particularly, the composition and distribution of mineral assemblages shift in both stable and radiometric isotope abundances, and the composition and filling temperatures of fluid inclusions should reflect the style and duration of fluid circulation. However, these data must have been collected with cognizance of the system's flow channels.

Fluids circulate from one rock, temperature, and pressure environment into another along pathlines defined by the fluid potential field and through fracture controlled channels. The fluid flux ranges from 10^{-4} to 10^{-8} gr^{-2} sec^{-1}, and the surface area of minerals exposed along the flow channels is relatively large compared to the amount of fluid in the flow channel. Recalling the porosity model of Norton and Knapp (1977), it is apparent that the circulating bulk fluid may be in direct contact with

between fluid and rock. The amount of fluid flowing through rock volume, V, is

$$M_f = \int_{t_1}^{t_2} A\bar{v}\rho_f dt, \tag{63}$$

where A is the cross-sectional area of the rock volume that is normal to the Darcy velocity vector, $\bar{v}$. The fluid-rock mass ratio in this case is defined by

$$\frac{M_f}{M_r} = \frac{\int_{t_1}^{t_2} A\bar{v}\rho_f dt}{\rho_r V}. \tag{64}$$

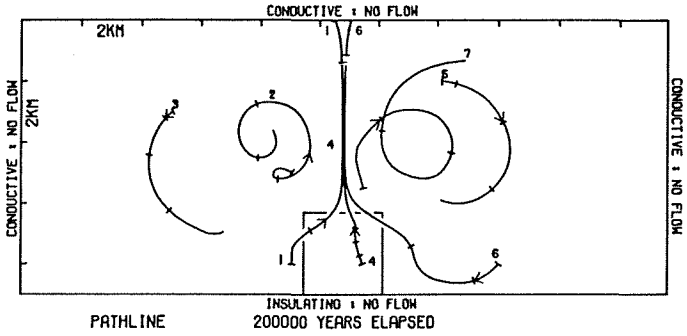

Fig. 32. Examples of fluid pathline in system P7 representing the redistribution of fluids caused by the thermal anomaly. Arrows indicate direction of fluid motion; tic marks occur every 5×10^4 yrs.

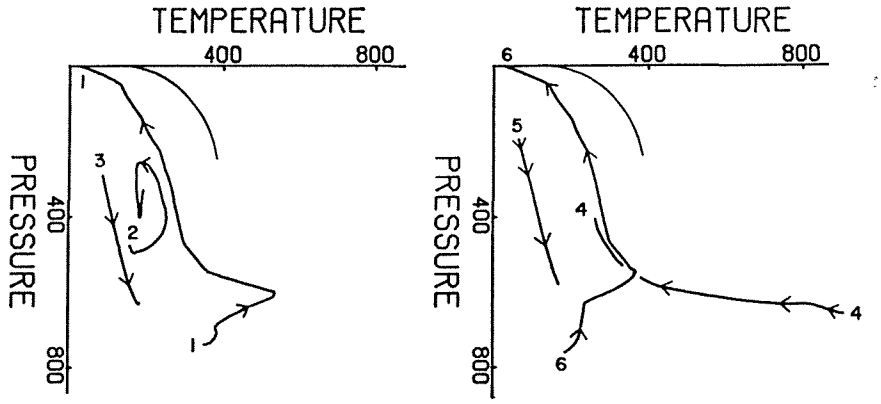

Fig. 33. Pressure-temperature path of fluid packets that circulate along paths in system P7 (fig. 32). Paths are shown with respect to liquid-vapor surface in H_2O system.

only a small portion of the rock in the permeable media, but the mass of fluid to rock ratios is large. As a consequence of the above features, the fluids being redistributed in natural systems will be grossly out of equilibrium with the bulk rock as they flow along the pathlines, although they may have initially been equilibrated with the bulk rock at their initial location. Therefore, if the overall irreversible nature of the reactions between circulating fluids and rocks, the nature of fracture controlled permeability, and the magnitude and direction of fluid flux are accounted for, the geochemical history of pluton environments can be defined.

Hydrothermal alteration phases and stable light isotope distributions have already been interpreted as indicating a style of fluid circulation similar to that indicated by our physical analysis (Helgeson, 1970; Taylor, 1971; and Norton, 1972). Indications that other chemical data may reflect this circulation process are evident. We wish to call attention to the fact that although shifts in chemical composition do indicate fluid redistribution and that in certain instances the direction of fluid flow can be implied, ultimately fluids are shifted into chemical equilibrium with the mineral phases along the flow channel. Subsequently, the fluid and mineral chemistry will not reflect a chemical shift in all or any of the chemical parameters.

Fluid circulation may have played a significant role in regions of the crust where magmatic and volcanic activity is most voluminous, such as along the crustal plate boundaries. The tectonic setting of both convergent and divergent plate boundaries is such that abundant fracturing of host rocks typically accompanies the igneous events. As a result, these environments probably have sufficiently large permeabilities to permit fluid circulation. Fluid circulation, total heat flux, and, consequently, the heat transfer through Earth's crust may be significantly greater than heretofore recognized. One manifestation of this voluminous fluid circulation is the large thicknesses of volcanic rocks that have been hydrothermally altered. Very clearly, our notions of heat flux are in error by perhaps as much as a factor of ten at plate boundaries, since geophysical surveys have probably not measured the convective component.

The divergent plate environment along oceanic ridges is an equally dramatic example of the potential significance of fluid circulation. Consider that the rate of seafloor spreading is proportional to the mass of igneous melt emplaced at the spreading center and further hypothesize that only the upper 2 km of the ridge environment has a permeability greater than 10^{-14} cm^2. Then, by analogy to the models presented above, a mass of fluid equivalent to the entire ocean system has been circulated through the spreading centers, over 2×10^8 yrs, if one assumes an average of 5 cm are added to the crust every year along the strike length of the mid-ocean ridges.

Finally, igneous bodies have interacted with a quantity of fluid nearly equivalent to their mass since permeabilities $\geqq 10^{-14}$ cm^2 appear to be reasonable values for many plutons in the shallow crust.

ACKNOWLEDGMENTS

This research was supported by NSF Grants GS-41136 and EAR74-03515 A01 and by matching computer funds from the University of Arizona Computer Center. Additional funds were provided in the early stages by the Universities of Utah and Arizona. The study has benefited from the suggestions and assistance from many of our colleagues, but in particular we are indebted to R. Knapp, R. N. Villas, T. Gerlach, H. Hardee, and D. W. Larson. The study was conceived when H. C. Helgeson pointed out that an early cartoon drawn by the principal author could be quantified, and the study has continually benefited from his critical comments. We are also grateful to H. C. Helgeson and David Kirkham for providing programs to compute equation of state properties in the H_2O–system. We wish to acknowledge the guidance from Lawrence Cathles during the early stages of program development. We wish to thank Lynn McLean for many improvements in the manuscript.

REFERENCES

Bear, Jacob, 1972, Dynamics of fluids in porous media: New York, Am. Elsevier, 764 p.

Bianchi, L., and Snow, D. T., 1969, Permeability of crystalline rocks interpreted from measured orientations and apertures of fractures: Jodphur, Rajasthan, Arid Zone Research Assoc. of India, Annals of Arid Zone, v. 8, no. 2, p. 231-245.

Bénard, M., 1901, Les tourbillons cellulaires dans une nappe liquide transportant de la chaleur par convection en régime permanent: Am. Chim. Phys., v. 23, p. 62-144.

Bruges, E. A., Latto, B., and Ray, A. K., 1966, New correlations and tables of the coefficient of viscosity of water and steam up to 1000 bar and 1000°C: Internat. Jour. Heat and Mass Transfer, v. 9, p. 465-480.

Clark, S. P., Jr., ed., 1966, Handbook of Physical Constants, rev. ed.: New York, Geol. Soc. America Mem. 97, 587 p.

Donaldson, I. G., 1962, Temperature gradients in the upper layers of the earth's crust due to convective water flows: Jour. Geophys. Research, v. 67, no. 9, p. 28-48.

———— 1968, The flow of stream water mixtures through permeable beds: a simple simulation of a natural undisturbed hydrothermal region: New Zealand Jour. Sci., v. 11, no. 1, p. 3-23.

Elder, J. W., 1965, Physical processes in geothermal areas, *in* Lee, W. H. K., ed., Terrestrial Heat Flow: Am. Geophys. Union, Geophys. Mon. Ser. 8, 276 p.

———— 1967, Steady free convection in a porous medium heated from below: Jour. Fluid Mechanics, v. 27, p. 29-84.

Helgeson, H. C., 1970, A chemical and thermodynamic model of ore deposition in hydrothermal systems: Mineralog. Soc. America Spec. Paper 3, p. 155-186.

Helgeson, H. C., and Kirkham, D. H., 1974a, Theoretical predictions of the thermodynamic behavior of aqueous electrolytes at high pressures and temperatures; I: Summary of the thermodynamic/electrostatic properties of the solvent: Am. Jour. Sci., v. 274, p. 1089-1198.

———— 1974b, Theoretical predictions of the thermodynamic behavior of aqueous electrolytes at high pressures and temperatures; II: Debye-Huckel parameters for activity coefficient and relative partial molal properties of the source: Am. Jour. Sci., v. 274, p. 1199-1261.

Holst, P. H., and Aziz, K., 1972, Transient three-dimensional natural convection in confined porous media: Internat. Jour. Heat and Mass Transformation, v. 15, p. 73-90.

Jaeger, J. C., 1968, Cooling and solidification of igneous rocks, *in* Hess, H., ed., Basalts, v. II: New York, John Wiley & Sons, Inc., p. 504-535.

Keenan, J. H., and Keyes, F. G., 1969, Steam Tables: New York, John Wiley & Sons, 162 p.
Lindgren, W., 1907, The relation of ore deposition to physical conditions: Econ. Geology, v. 2, p. 105-127.
Lister, C. R. B., 1974, On the penetration of water in hot rock: Astron. Soc. Jour. Geophys. Research, v. 39, p. 465-509.
Lovering, T. S., 1935, Theory of heat conduction applied to geological problems: Geol. Soc. America Bull., v. 46, p. 69-94.
Nield, D. A., 1968, Onset of thermohaline convection in a porous medium: Water Resources Research, v. 4, p. 553-560.
Norton, D., 1972, Concepts relating anhydrite deposition to solution flow in hydrothermal systems: Internat. Geol. Cong., 24th, Montreal 1972, sec. 10, p. 237-244.
Norton, D., and Knapp, 1977, Transport phenomena in hydrothermal systems: The nature of rock porosity: Am. Jour. Sci., v. 277, p. 913-936.
Peaceman, D. W., and Rachford, H. H., Jr., 1955, The numerical solution of parabolic and elliptic differential equations: Soc. Indust. Appl. Math. Jour., v. 3, no. 1, p. 28-41.
Rayleigh, Lord, 1916, On convection currents in a horizontal layer of fluid, when the higher temperature is on the underside: Philos. Mag., ser. 6, v. 32, p. 529-545.
Ribando, R. J., Torrance, K. B., and Turcotte, D. L., 1976, Numerical models for hydrothermal circulation in the oceanic crust: Jour. Geophys. Research, v. 81, p. 3007-3012.
Roache, Patrick J., 1972, Computational Fluid Dynamics: Albuquerque, N.M., Hermosa Publishers, 434 p.
Rubin, H., 1973, Effect of nonlinear stabilizing salinity profiles on thermal convection in a porous medium layer: Water Resources Research, v. 9, p. 211-221.
Schmidt, E., 1969, Properties of Water and Steam in SI-Units: New York, Springer-Verlag, 205 p.
Ssu-hsiao, C., 1250, *in* Brower, ed., Of All Things Most Yielding: San Francisco, California, McGraw Hill, Friends of the Earth, 128 p.
Taylor, H. P., Jr., 1971, Oxygen isotope evidence for large-scale interaction between meteoric ground waters and Tertiary granodiorite intrusions, Western Cascade Range, Oregon: Jour. Geophys. Research, v. 76, p. 7755-7873.
Van Hise, C. R., 1901, Some principles controlling the deposition of ores: Am. Inst. Min. Eng. Trans., v. 30, p. 27.
Veronis, G., 1968, Effect of stabilizing gradient of solute on thermal convection. Jour. Fluid Mech., v. 34, p. 315-336.
Villas, N. R., ms, 1975, Fracture analysis, hydrodynamic properties, and mineral abundance in altered igneous rocks at the Mayflower Mine, Park City District, Utah: Ph.D. dissert., University of Utah, Salt Lake City, 253 p.
Wooding, R. A., 1957, Steady state free thermal convection of liquid in a saturated permeable medium: Jour. Fluid Mech., v. 2, p. 273-285.